THE PUMPING OF BENTONITE CLAYS

by

© GARY ARTHUR DAVIDSON, B. Eng.

A Thesis

Submitted to the Faculty of Graduate Studies

in Partial Fulfilment of the Requirements

for the Degree

Master of Engineering

McMaster University

September 1979

THE PUMPING OF BENTONITE CLAYS

MASTER OF ENGINEERING (1979) McMASTER UNIVERSITY
(Mechanical Engineering) Hamilton, Ontario.

TITLE: The Pumping of Bentonite Clays

AUTHOR: Gary Arthur Davidson
B. Eng.,
McMaster University.

SUPERVISOR: Dr. B. Latto

NUMBER OF PAGES: xiv, 156

ABSTRACT

This study describes the results of experiments on the pumping of non-Newtonian bentonite clay slurries. The data were obtained from smooth tubes having internal diameters of 0.60 cm, 1.27 cm and 1.74 cm, for aqueous suspension concentrations of 1.96, 4.0, 5.0, 6.0 and 8.0% by weight. The flow Reynolds numbers varied to a maximum of about 6000.

Shear stress-shear rate curves were obtained as well as apparent viscosity and generalized Bingham plastic plots. Specific power was plotted against Reynolds number for all concentrations. It was found in general that the data of the shear curve agreed quite well with that from other sources but that there were discrepancies for the Bingham plastic equation. The fact that Newtonian friction factor curves for flow in smooth pipe can be used in conjunction with bentonite slurries in an equilibrium state was also demonstrated.

ACKNOWLEDGEMENTS

The author wishes to express his sincere appreciation to Dr. B. Latto and Dr. G. F. Round whose continued encouragement made the completion of this work possible.

For their technical assistance during the construction of the experimental apparatus, Mr. D. Schick and Mr. F. Drieman receive the author's deepest gratitude.

TABLE OF CONTENTS

LIST OF FIGURES

LIST OF TABLES

NOTATION

a	internal pipe radius
A	fluid constant in Williamson equation
α	area
B	fluid constant in Williamson equation
c	$=\tau_y/\tau_w$ as defined by Weltmann (1956)
C	concentration by weight
C_f	Fanning friction factor $= \left(\frac{D\Delta P}{4L} \Big/ \frac{\rho u_m^2}{2}\right)$
D	internal pipe diameter
$\frac{D}{Dt}$	total derivative $= u_x\frac{\partial}{\partial x} + u_y\frac{\partial}{\partial y} + u_z\frac{\partial}{\partial z} + \frac{\partial}{\partial t}$
$-(du/dr)$	velocity gradient in laminar pipe flow
$-(du/dr)_w$	rate of shear at pipe wall or boundary
∇^2	$=\frac{\partial^2}{\partial x^2} + \frac{\partial^2}{\partial y^2} + \frac{\partial^2}{\partial z^2}$
f	denotes functional relationship
g	acceleration due to gravity = 9.81 $m \cdot s^{-2}$
g_c	universal gravitational constant = 1.00 $kg \cdot m \cdot s^{-2}$
G	constant in generalized von Karman equation of Dodge and Metzner (1959)
G'	$= R\log\left[(1/8)\ (6n'+2/n')^{n'}\right] + G$
$\dot{\gamma}$	shear rate
$\dot{\gamma}_o$	extrapolated dilatant shear rate at $\tau=0$
He	Hedstrom number = Re*S

J	time coefficient of thixotropic breakdown $= (\mu_1-\mu_2)/\ln(t_2/t_1)$
k	consistency coefficient in power law equation and generalized Bingham equation
k'	coefficient in generalized power law equation of Metzner and Reed (1955)
L	length
L_e	entrance length
M	coefficient of thixotropic breakdown
μ	viscosity
μ_a	apparent viscosity
μ_p	coefficient of rigidity (plastic viscosity)
μ_o	limiting viscosity at zero shear rate
μ_∞	limiting viscosity at infinite shear rate
μ_1, μ_2	plastic viscosities at t_1 and t_2 as defined by Weltmann (1943)
n	shear rate index in power law equation and generalized Bingham equation
n'	flow index in Mooney equation developed by Metzner and Reed (1955) $= d(\ln D\Delta P/4L)/d(\ln 8u_m/D)$
P	pressure
ΔP	pressure differential
π	pi = 3.14159
q	volumetric flow rate
Q	power
r	radius

r_p	radius of unsheared plastic plug in pipe flow
R	coefficient in generalized von Karman equation of Dodge and Metzner (1959)
Re	Reynolds number = $\rho D u_m / \mu$
Re'	generalized Reynolds number defined by Metzner and Reed (1955)
Re^o	$= D^n u_m^{2-n} \rho / k$ (Dodge and Metzner, 1959)
Re^*	limiting Reynolds number
ρ	density of fluid or slurry
S	plasticity number = $\tau_y D / \mu_p u_m$
t	time
t_1, t_2	times of shear duration as defined by Weltmann (1943)
T	torque
τ	shear stress
τ_w	wall shear stress
τ_y	yield shear stress
τ_o	extrapolated pseudoplastic yield value at zero $\dot{\gamma}$
τ_1, τ_2	shear stresses at times t_1 and t_2
θ	temperature
u	velocity
u_m	mean fluid velocity
u_p	velocity of unsheared central core in Bingham plastic pipe flow
v	volume

V	coefficient of thixotropic breakdown
ω	rotational speed
ω_1, ω_2	rotational speeds at times t_1 and t_2
X	component of body force
x, y, z	denote orthogonal Cartesian coordinate directions
50/50 kerosene in 10W40	denotes mixture of 50% kerosene and 50% SAE 10W40 motor oil by volume

CHAPTER 1

INTRODUCTION AND LITERATURE REVIEW

1.1 Introduction

A fluid is said to be Newtonian if its viscosity is solely a function of pressure and temperature, and non-Newtonian otherwise. Non-Newtonian fluids make up a large portion of those handled by industry, yet the theory which quantifies their characteristics is still rather underdeveloped, a primary reason being the inability to produce a generally accepted rheological equation of state which satisfactorily describes the system and is convenient to work with.

Non-Newtonian fluids are subdivided into three groups depending on the functional relation between shear stress, shear rate and time. They are called time-independent when the rate of shear is a function of shear stress only, time-dependent when the rate of shear is additionally a function of the time for which the stress has been applied and viscoelastic if the material exhibits elastic recovery after being deformed.

With increased concern to minimize the energy input required to transport various fluids in pipes it becomes especially necessary to understand and be able to predict the behaviour of non-Newtonian fluid flow. It

was the purpose of this study to investigate the flow of non-Newtonian bentonite clay slurries in a model pipe line system.

1.2 Rheology of Newtonian Fluids

Viscosity is defined by the slope of the shear diagram (plot of τ vs. $\dot{\gamma}$) and is constant for a Newtonian fluid provided the shearing is done isothermally at constant pressure. The relation between shear stress and shear rate in laminar pipe flow can be expressed as follows:

$$\tau = -\mu du/dr = \mu\dot{\gamma} \qquad (1.1)$$

The relationship between flow rate and pressure drop for the laminar flow of Newtonian fluids in smooth circular pipes can readily be derived from the Navier-Stokes equation for the axial direction of the pipe in cylindrical coordinates. This can be written as:

$$\frac{\rho Du_z}{Dt} = \rho X_z - \frac{\partial P}{\partial Z} + \mu\nabla^2 u_z$$

This readily reduces to the familiar Hagen-Poiseuille equation:

$$q = \pi a^4 \Delta P/8\mu L \qquad (1.2)$$

The shearing stress at any radius r in Hagen-Poiseuille flow can be shown to be:

$$\tau = r\Delta P/2L$$

and at r = a, the pipe wall, the shear stress is denoted by

τ_w:

$$\tau_w = a\Delta P/2L \qquad (1.3)$$

Shear diagrams are generally plotted in terms of the consistency variables $a\Delta P/2L$ and $4q/\pi a^3$. The slope of this line for a Newtonian fluid is now given by:

$$\mu = \pi a^4 \Delta P/8Lq \qquad (1.4)$$

Measurements made for the same fluid in pipes of various lengths and diameters should fall on the same curve if plotted in this fashion (Reiner, 1949). This result can be used to a good approximation for non-Newtonian fluids provided they are not time dependent (Alves et al. 1952).

Newtonian behaviour is generally exhibited by fluids comprised of comparatively small molecules whose collisions are elastic in nature rather than interactive. Gases, liquids and suspensions of low molecular weight are included although there are exceptions of colloidal suspensions and polymeric solutions where the molecular species are large (Wilkinson, 1960). In most cases Newtonians are one-phase systems and therefore often well defined and easily reproducible (Hedstrom, 1952).

1.3 Rheology of Time-Independent Non-Newtonian Fluids

i) Bingham Plastics

Bingham plastics are characterized by a shear diagram which is linear and has an intercept τ_y (Fig. 1.1) on the

shear stress axis (Bingham and Green, 1919). The yield stress τ_y, is the stress which must be exceeded before flow commences. The rheological equation for a Bingham plastic may be written as:

$$\tau - \tau_y = \mu_p \dot{\gamma} \quad , \quad \tau > \tau_y \qquad (1.5)$$

where μ_p is called the plastic viscosity or coefficient of rigidity and is the slope of the shear diagram.

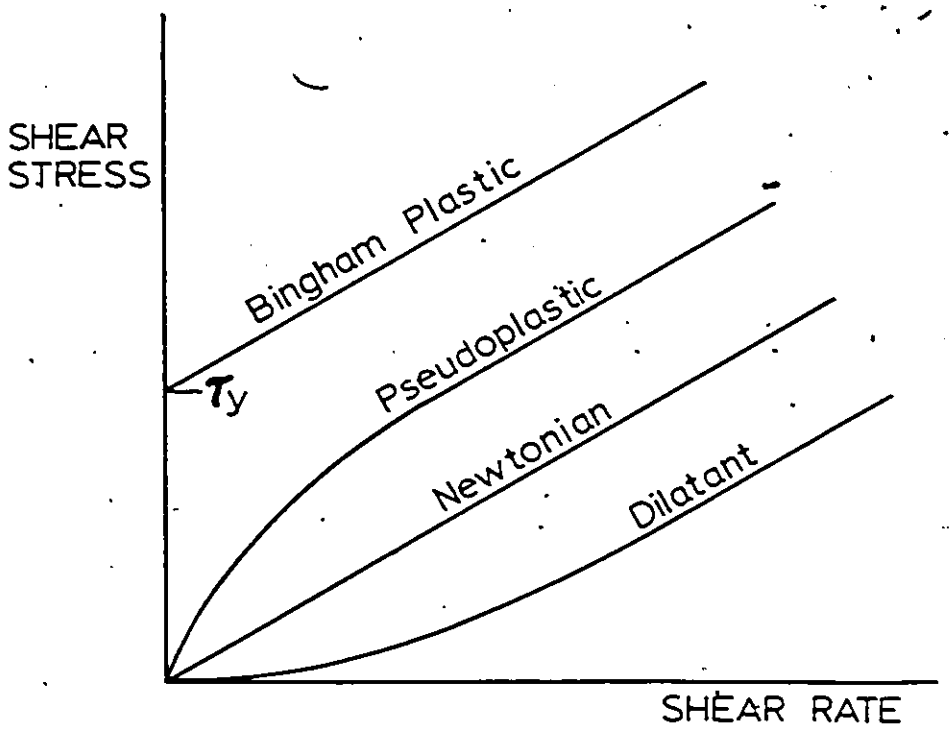

Figure 1.1 Shear diagrams for time-independent non-Newtonian fluids

Many real fluids such as slurries, drilling muds, paints, toothpaste and sewage sludges closely approximate Bingham plastics. At rest, the structure of the material is sufficiently rigid to resist flow under any stress less than τ_y. Once the yield stress is exceeded, the structure completely breaks down and the system behaves as if it were a Newtonian fluid under a shear stress $\tau-\tau_y$.

For a Bingham plastic, equation (1.5) can be rewritten as:

$$-du/dr = (\tau-\tau_y)/\mu_p = f(\tau); \quad \tau_y<\tau<\tau_w$$

Since $\tau = r\Delta P/2L$ at any radius r, then (1.5) can be rearranged to give:

$$du = \frac{-1}{\mu_p}\left[\frac{r\Delta P}{2L} - \tau_y\right]dr$$

The velocity at any distance r from the center of the pipe to the pipe wall is obtained by integration from r = a to r = r.

$$\int_a^r du = \frac{-1}{\mu_p}\int_a^r \left[\frac{r\Delta P}{2L} - \tau_y\right]dr$$

$$\therefore u(r)-u(a) = \frac{1}{\mu_p}\left(\left[\frac{r^2\Delta P}{4L} - \tau_y r\right]_r^a\right)$$

assuming no slip at the wall:

$$u(r) = \frac{1}{\mu_p}\left[\frac{(a^2-r^2)\Delta P}{4L} - \tau_y(a-r)\right] \qquad (1.6)$$

is the velocity distribution for flow in a tube of radius a (Fig. 1.2).

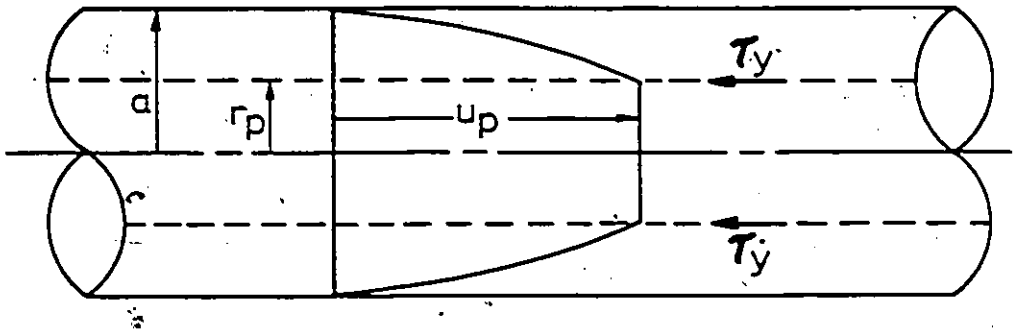

Figure 1.2 Velocity profile for a Bingham plastic flow

In a viscous liquid the shearing stress vanishes at the axis of the pipe and increases with distance from it. Therefore, around the axis there will be a cylinder of material in which $\tau < \tau_y$. The shearing stresses in this cylinder will be elastic in nature and the cylinder will move as a solid central plug, hence the term 'plug flow'. At the surface of this central core, the shear will be equal to the yield value τ_y of the material.

Let r_p be the radius of the central core. Thus:

$$\tau_y = r_p \Delta P / 2L \qquad (1.7)$$

Where $r = r_p$, $du/dr = 0$; thus for $r < r_p$ while there is movement, there is no flow (flow requiring relative motion between adjacent fluid layers). The velocity of the plug u_p, is found by introducing into (1.6) r_p for r and for τ_y the

value from (1.7). Thus:

$$u_p = \Delta P/4L\mu_p \ (a-r_p)^2 \qquad (1.8)$$

In principle, given the shear diagram, the relation between pressure drop and flow rate may be derived for any fluid by the numerical integration of the empirical expression for $f(\tau)$ using the following equation (Wilkinson 1960):

$$q/\pi a^3 = 1/\tau_w^3 \int_0^{\tau_w} \tau^2 f(\tau) \ d\tau \qquad (1.9)$$

In the case of non-Newtonian fluids it is the determination of the functional dependence of τ on $\dot{\gamma}$ which is of primary interest since the relations are usually difficult to integrate (Thomas, 1962). However, for a Bingham plastic, equation (1.9) is easily integrated if $f(\tau)$ is given by (1.5); that is:

$$q/\pi a^3 = 1/\mu_p \tau_w^3 \int_{\tau_y}^{\tau_w} \tau^2 (\tau-\tau_y) \ d\tau$$

$$= \tau_w/\mu_p \left[1/4-1/3(\tau_y/\tau_w)+1/12(\tau_y/\tau_w)^4\right]$$

substitution for τ_w yields:

$$q = \frac{\pi a^4 \Delta P}{8L\mu_p}\left[1 - \frac{4}{3}\left(\frac{2L\tau_y}{a\Delta P}\right) + \frac{1}{3}\left(\frac{2L\tau_y}{a\Delta P}\right)^4\right] \qquad (1.10)$$

This equation was developed independently by both Buckingham (1921) and Reiner (1949) and is known as the Buckingham-Reiner equation for Bingham plastics. It re-

duces to the Hagen-Poiseuille equation for Newtonian flow when $\tau_y = 0$.

Caldwell and Babbitt (1941) have successfully applied the Buckingham-Reiner equation to the flow of muds and sludges. They did a theoretical analysis of flows in circular pipes and distinguished two types of flow termed 'plastic' and 'turbulent' depending upon the flow rate. An equation for determining the 'critical velocity' at which plastic flow changes to turbulent flow was also presented, along with equations for turbulent flow. The mean velocity of the flow was developed in the form of the Buckingham-Reiner equation to give:

$$u_m = gD\tau_w/8\mu_p \left[1-4/3(\tau_y/\tau_w)+1/3(\tau_y/\tau_w)^4\right] \qquad (1.11)$$

Caldwell and Babbitt assert that the last term may be omitted with little error when $\tau_y/\tau_w < 0.5$. McMillen (1948) contends that this cannot be done without introducing significant errors since his values of τ_y/τ_w for plastic gels of an aluminum soap dispersed in a petroleum fraction were all greater than 0.5 for flow conditions of practical interest.

If τ_w is plotted versus $8u_m/gD$, the slope of the resulting curve gives μ_p, and the intercept will give a value of τ_w which is 4/3 of τ_y.

McMillen (1948) simplified the computations for

Bingham plastic flow by developing the Buckingham-Reiner equation in terms of the central unsheared plug radius r_p, and the pipe radius a. The equations are then expressed in terms of dimensionless quantities, (r_p/a) and (r/a) as well other dimensionless parameters derived from these two. Values of dimensionless quantities which are functions of the relative plug radius, r_p/a, can be evaluated and presented graphically for design purposes. A maximum Reynolds number in terms of these dimensionless groups was developed and is the basis for determining the onset of turbulence. The viscosity at the fluid layer under consideration, rather than a mean viscosity for the plastic material from the wall to that point was assumed to be the proper viscosity to use in computing Reynolds number.

In order to make use of the various dimensionless quantities in the equations, it is necessary to know τ_w and μ_p. These may be obtained from linear pressure drop determinations at two flow rates in a pipe of any diameter. Obviously several determinations would improve accuracy.

Wilhelm, Wroughton and Loeffel (1939) developed a friction factor-Reynolds number diagram for cement rock suspensions which yielded a series of straight lines with sharp negative slopes. However, it was not until Hedstrom (1952) published a paper on the flow of plastics in pipes that their data were substantiated by a theoretical analysis.

Hedstrom proposed a simple criterion for distinguish-

ing between laminar and turbulent flows using dimensional analysis of the Buckingham-Reiner equation which produced the following non-dimensional 'Hedstrom' group:

$$He = Re^*S = (D\rho u_m/\mu_p)(\tau_y D/\mu_p u_m)$$

$$= \rho\tau_y D^2/\mu_p = \text{constant} \qquad (1.12)$$

He also presented values of 'He' for the cement rock data of Wilhelm et al. on a friction factor diagram. In the laminar region, the slope of the curves approached a value of -2 as S approached infinity, however as S decreased they approached -1; S indicates the degree of plastic behaviour. The He curves in all cases followed closely the experimental curves for the laminar region, indicating that the material appeared to be a Bingham plastic. In the turbulent region the data agreed closely with standard Newtonian friction factor curves for smooth pipes. Hedstrom postulated that the turbulent friction curve is applicable for both Newtonian and plastic liquids and that turbulence commences at conditions when the He and Newtonian C_f curves intersect.

In summary, although the Buckingham-Reiner equation cannot be solved for q or ΔP explicitly, several methods are available for correlating pipe flow data of plastics either graphically or in a non-dimensional manner to simplify the use of this equation.

ii) Pseudoplastics

Pseudoplastic fluids have no apparent yield stress and the typical shear diagram (Fig. 1.1) for these materials indicates that the slope decreases continuously with shear rate until a point is reached at higher rates of shear where the curve becomes linear.

In many cases the logarithmic plot of the shear diagram is linear with a slope less than one and as a result pseudoplastics can be characterized by a power law relation of the form:

$$\tau = k\dot{\gamma}^n \qquad (1.13)$$

k being a measure of the consistency of the fluid; large values of k indicate a viscous fluid and n is a measure of how non-Newtonian the fluid is (the greater n's divergence from unity, the more emphatic are the fluid's non-Newtonian characteristics). Furthermore, n is not constant over all possible ranges of shear, and a representative value of n for the range under consideration is usually used (Reiner, 1949).

From the definition of apparent viscosity (see Appendix A for a brief discussion of viscosity) it is seen that for a power law fluid:

$$\mu_a = \tau/\dot{\gamma} = k\dot{\gamma}^{n-1}$$

and since $n<1$ for pseudoplastics, it is obvious that the

apparent viscosity decreases as the rate of shear increases.

Suspensions of asymmetric particles or polymer solutions, such as cellulose derivatives exhibit pronounced degrees of pseudoplasticity. Wilkinson (1960), gives a physical explanation of this phenomenon by postulating that as the shear rate is increased, the asymmetric particles or molecules become aligned with their longitudinal axes parallel to the direction of flow. The apparent viscosity will continue to decrease with increasing rate of shear until no further particle alignment is possible at which point the shear diagram will become linear. The alignment of molecules must take place instantaneously (or at least fast enough to not be detected) or the fluid is no longer classified as time independent.

An alternative explanation for pseudoplasticity is based on the distortion of an oriented structure under an applied stress (Winding et al. 1947[1]). Work must be done to disintegrate the structure and the molecules must rearrange themselves when the stress is removed. This should not be confused however with the time dependent phenomenon of thixotropy.

Winding, Baumann and Kranich (1947[1]) used the Williamson equation (Williamson, 1929) to model the flow of pseudoplastic latex materials:

$$\tau = A\dot{\gamma}/(B+\dot{\gamma}) + \mu_\infty \dot{\gamma}$$

This equation implies that the power required to shear a

pseudoplastic is comprised of the power required to cause ordinary laminar flow and an additional amount to deform and/or deflocculate aggregates. Strictly speaking, the theoretical background for the equation was developed for shear between two infinite parallel plates where the stress gradient is constant, but the form of the equation is useful for pipe flow.

They carried on to extrapolate data from capillary tube viscometers for the prediction of laminar and turbulent flow in commercial size pipes. (Winding et al. 1947[2]). Since the apparent viscosity varies with rate of shear across the flow as well as with the overall volume rate of flow, it must be realized that Reynolds number has no true meaning in pseudoplastic flow. Winding et al. found that when drawing the friction factor-Reynolds number diagram for highly pseudoplastic materials in pipe flow, it was best to use μ_o in the calculation of Re to get reasonably good correlations in the laminar region. However in turbulent flow it was found that the substitution of μ_∞ into Re gave the best correlations and data from different size pipes fell closer together near the Newtonian curve.

In summary, if a power law equation cannot be used conveniently, Winding et al. propose that for a material of low pseudoplasticity, flow relations may be computed using the Hagen-Poiseuille or Fanning equation if μ_o is the sub-

stituted viscosity. If estimates to a higher degree of accuracy are required in the laminar region, the Williamson equation can be applied. In the turbulent region, the graph of C_f vs. Re can be constructed using the limiting viscosity at infinite shear in the computation of Re.

iii) Dilatant Materials

Like pseudoplastics, dilatant materials show no yield stress, but the apparent viscosity for these materials increases with increasing rates of shear. Once again, the power law relation (1.13) is often used to describe the flow characteristics of these systems and the exponent n, is now greater than unity. Dilatancy was first investigated by Osborne Reynolds (1896) as he performed experiments on concentrated sand-water suspensions. He postulated that when these suspensions are sheared at low rates, there is sufficient lubrication of the particles past each other by the liquid medium to maintain the shear stresses at a low value. Upon increasing the shear rate, the tight packing of the particles is disrupted and expansion or volumetric dilation occurs subsequently increasing the voidage. There is no longer enough liquid to completely fill the voids and lubricate the flow of particles past each other, thereby magnifying the applied shear stresses. This in turn causes a significant increase in apparent viscosity.

In general, the term dilatancy has been used inter-

changeably to describe both of the above phenomena, sometimes implying that volumetric dilation under shear is accompanied by substantial increases in apparent viscosity. It has been pointed out however (Metzner and Whitlock, 1958) that volumetric dilation may occur quite separately from dilatancy in the rheological sense (ie. increased apparent viscosity).

Freundlich and Roder (1938) had previously studied starch-water and quartz-water suspensions which did not dilate on shearing in the normal sense of the word but are still referred to as dilatant because of the increase in viscosity. Verwey and deBoer (1939) studied dilatant suspensions of metallic particles. Both investigations concluded that dilatant behaviour occurred only over very narrow concentrations ranges. Verwey and deBoer present an explanation for dilatancy based upon electrical attraction of the particles. When a substance such as oleic acid was added to the suspension, the electrical properties were altered and the suspension flowed more freely.

Metzner and Whitlock (1958) studied titania suspended in water and aqueous sucrose, concluding that all systems exhibit dilatancy after reaching a certain titania concentration (more dilute solutions were essentially Newtonian in behaviour). They found that shear diagrams for many of the dilatant suspensions took the general form shown in Fig. 1.3. This observation is supported by Hoffman (1972).

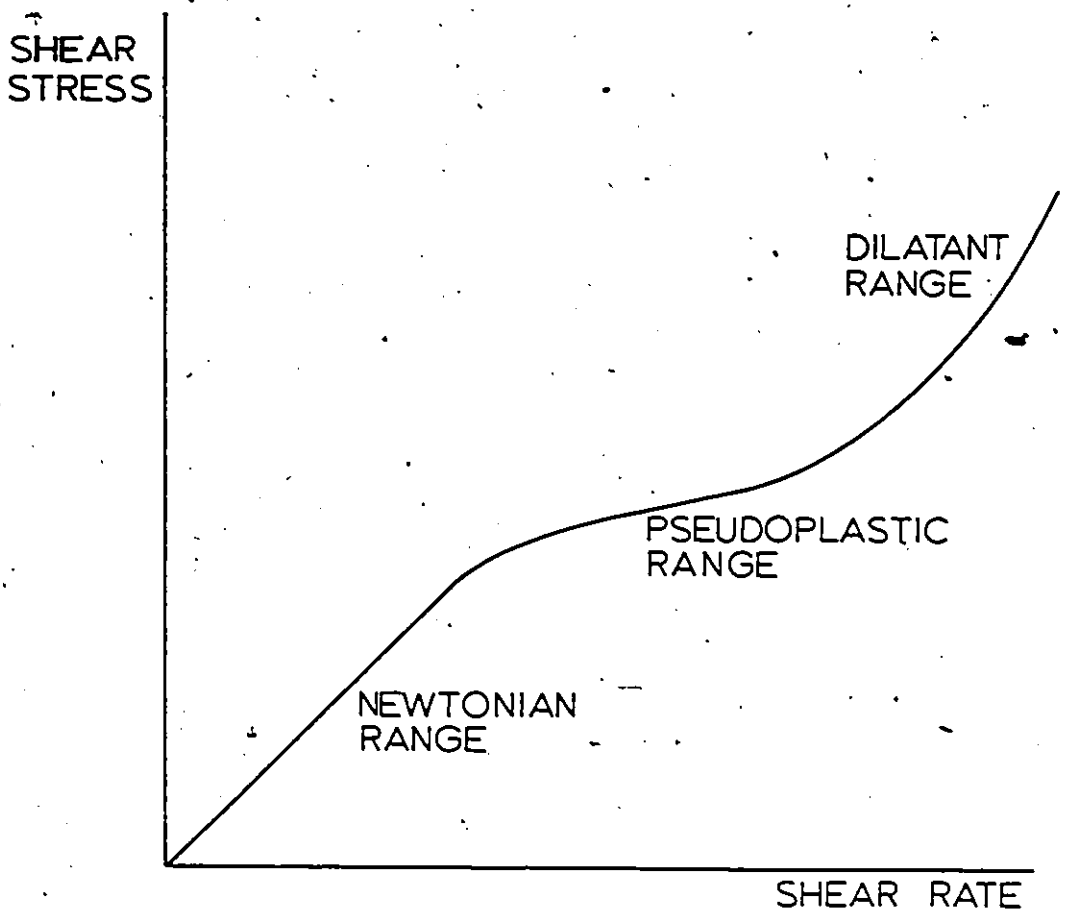

Figure 1.3 General shape of shear diagram for dilatant suspensions (after Metzner and Whitlock, 1958)

At low shear rates Newtonian behaviour is predominant in the absence of sufficient forces to affect either particle size or alignment. At moderate shear rates the slope of the curve drops off as the flowing particles either align (if asymmetric) or are deflocculated due to the imposing shear forces (pseudoplastic range). Two mechanisms may account for the inflection and subsequent increase in slope of the curve:

1. Once the shearing forces have become large enough

that they reduce the flocculates to a minimum size, the viscosity should remain fairly constant.

2. Agitation of the particles at high shear stresses does not allow them to remain close packed (volmetric expansion) hence the flow mechanism begins to change to one in which entire layers of particles begin to glide over adjacent layers (Reiner, 1929).

Time independent non-Newtonian fluids of the Bingham plastic and pseudoplastic type have been studied quite extensively and most of the progress in characterizing these fluids has been made by extending simple Newtonian flow concepts to account for the peculiarities of the particular systems. Rheological models of the Bingham plastic and power law form are simple and fairly easy to work with. More complicated models can be generated to increase accuracy of computations if the need arises.

1.4 Universal Pipe Line Correlations

In order to simplify engineering design procedures, a universal pipe line correlation which could be applied to any time-independent fluid equally well has been sought.

Alves, Boucher and Pigford (1952) took advantage of the fact that for fluids with rheological properties independent of time the relationship between the consistency variables $a\Delta P/2L$ and $q/\pi a^3$ in the laminar region is unique and independent of pipe size (any discrepancy in the curves

may be due to anomalous flow behaviour, slip at the wall (Oldroyd, 1949) or time dependence). In the case of non-Newtonian solutions and suspensions they assert that the Hagen-Poiseuille equation (1.2) may be used by replacing μ with an apparent viscosity μ_a. The difficulty arises in determining μ_a accurately since it is not constant. A plant-scale pipe line can readily be sized once the shear diagram (in terms of consistency variables) is obtained from pipe line viscometer data provided the material is not time dependent. The Reynolds number ($\rho D u_m/\mu_a$) for the design case should be checked to see if it is greater than 2100 when the flow has become turbulent.

Correlations of pipe line and rotational viscometer data can also be made on the basis of comparing τ_w and $\dot{\gamma}$ at the pipe wall with those at the inner cylinder wall of the rotational viscometer. A plot of τ_w vs. $\dot{\gamma}$ at the inner cylinder wall can be prepared from a plot of T vs. ω (Reiner, 1929). For pipe line flow, a plot of $D\Delta P/4L$ vs. $8q/\pi D^3$ is prepared first. The rate of shear at the pipe wall is more difficult to evaluate. However, the following expression, called the Mooney-Rabinoswitsch equation (Mooney, 1931) can be applied to pipe line data:

$$-(du/dr)_w = 3(8q/\pi D^3)+(D\Delta P/4L) \\ * \; d(8q/\pi D^3)/d(D\Delta P/4L) \qquad (1.14)$$

Thus, the rate of shear at the pipe wall, $-(du/dr)_w$

can be obtained from this equation together with the plot of $D\Delta P/4L$ against $8q/\pi D^3$, where values of the abscissa and the slope can be obtained for selected values of $D\Delta P/4L$. Both pipe line and rotational viscometer data for a given material should fall on a single common curve when correlated in this manner, providing there is no time dependency.

Metzner(1954) has also proposed a general method for predicting the pipe line pressure drop requirements for laminar flow of time independent non-Newtonians. The basic assumptions of this development were:

1. The shear rate in a pipe was assumed to be a unique function of the ratio u_m/D.
2. The shear rate in a rotational viscometer was assumed to be a unique function of its rotational speed, ω.
3. The functional forms of both the relationships stated above are identical. If this is the case then the ratio of the shear rate in a pipe to that in a viscometer is a unique function of the dimensionless ratio $u_m/\omega D$ (although this has not been theoretically substantiated, Metzner does give experimental justification).

The viscosity obtained from the viscometer may be used directly in the Hagen-Poiseuille equation to obtain a calculated pressure drop ΔP_{calc}. This calculated pressure

drop can then be converted to the actual pressure drop in the pipe line (ΔP_{actual}) by means of the ratio of the shear rate in the pipe to that in the viscometer as expressed by the ratio $u_m/\omega D$. The functional relationship between the two dimensionless ratios $\Delta P_{calc}/\Delta P_{actual}$ and $u_m/\omega D$ is most conveniently determined graphically. In this way both the stress-strain relationships of the fluid and the dimensionless ratio $u_m/\omega D$ are kept constant during scale up from model to prototype; the former by using the identical fluid under identical conditions in both model and prototype, and the latter by operating the model with the same u_m/D as will be used in the prototype.

Metzner and Reed (1955) developed a more generalized method of correlating non-Newtonian pipe flow by rearranging the Mooney expression. Introducing the mean velocity, $u_m = 4q/\pi D^2$ equation (1.14) can be rewritten as:

$$-\left(\frac{du}{dr}\right)_w = \frac{3}{4}\left(\frac{8u_m}{D}\right) + \frac{1}{4}\left(\frac{8u_m}{D}\right)\frac{d\ln(8u_m/D)}{d\ln(D\Delta P/4L)}$$

Denoting the derivative by $1/n'$, this becomes:

$$-(du/dr)_w = (3n'+1)/4n'(8u_m/D) \qquad (1.15)$$

This form of the equation is an entirely general expression of the relationship between rate of shear, $(-du/dr)$ and bulk flow rate of the fluid. It is preferable to the original equation for two reasons:

1. It is a simpler more compact form.

2. The derivative, n' represents the slope of a logarithmic plot of $D\Delta P/4L$ vs. $8u_m/D$ and has been found to be very nearly a constant over wide ranges of shear stress for a great variety of non-Newtonian fluids and is therefore easier to work with.

One may write over any range of shear stresses for which n' is constant:

$$\tau_w = D\Delta P/4L = k'(8u_m/D)^{n'} \qquad (1.16)$$

It has been found experimentally that for most fluids k' and n' are constant over wide ranges of $8u_m/D$ or $D\Delta P/4L$ (Metzner and Reed, 1955). Thus from a logarithmic plot of $D\Delta P/4L$ vs. $8u_m/D$, n' and $8u_m/D$ can be determined for selected values of $D\Delta P/4L$. The corresponding rate of shear at the wall then follows from (1.15).

Substitution for $8u_m/D$ in (1.16) from (1.15) yields:

$$\tau_w = k'(4n'/3n'+1)(-du/dr)_w^{n'} \qquad (1.17)$$

If n' is a constant with the value of unity, this becomes:

$$\tau_w = k'(-du/dr)_w \qquad (1.18)$$

which is the familiar relation for a Newtonian fluid (k' becoming the Newtonian viscosity).

If on the other hand, n' is less than one (pseudoplastic fluid) or greater than one (dilatant), one obtains an equation similar to the power law equation (1.13):

$$\tau_w = k(-du/dr)^n \qquad (1.19)$$

and k' and n' are closely related to k and n.

Although equations (1.16) and (1.19) are similar, the former has some important advantages for engineering applications. It is, in fact, a direct relation between the pressure drop ΔP and the flow rate (or mean velocity) in terms of the tube dimensions and the characteristic parameters of the fluid k' and n'. Hence it may be used for a rigourous pipe line design provided k' and n' are known at the appropriate values of $8u_m/D$ under consideration. However if the power law (1.19) is used for pipe line design it must be integrated and this implies that the index n is constant over the whole range of shear stresses in the pipe (from $D\Delta P/4L$ at the wall to zero at the center). This is frequently not the case as pointed out previously (Reiner, 1949).

Metzner and Reed then go on to relate ΔP in equation (1.16) to the Fanning friction factor given as:

$$C_f = \frac{D\Delta P}{4L} \Big/ \frac{\rho u_m^2}{2} \qquad (1.20)$$

In order to use the conventional friction factor chart for Newtonian and non-Newtonian fluids alike in the laminar region it is convenient to let $C_f = 16/Re'$. The generalized Reynolds number (Re') is then found by combining (1.16) and (1.20) to give:

$$Re' = D^{n'} u_m^{2-n'} \rho / k' 8^{n'-1} \qquad (1.21)$$

which is dimensionless.

It must be emphasized that all fluids must follow the usual C_f vs. Re diagram in the laminar region when the generalized Reynolds number is used. If perfect coincidence with the laminar friction factor line is not achieved, either the data or the calculations are erroneous or the fluid exhibits time dependent behaviour.

In order to make use of these relationships, it is necessary to obtain k' and n' experimentally for a given fluid. The most suitable method is to measure a series of pressure drops and flow rates in laminar flow through a capillary tube viscometer and apply (1.16) to these data.

Weltmann (1956) suggests a similar correlation on the friction factor diagram by defining the Reynolds number as:

$$Re = \frac{\rho u_m D}{\text{'viscosity'}}$$

the viscosity being the Newtonian viscosity μ, for Newtonian fluids, the plastic viscosity μ_p, for Bingham plastics and the apparent viscosity under the given flow conditions for pseudoplastic and dilatant materials. The friction factor is related to Reynolds number in the conventional manner ($C_f = 16/Re$) for laminar Newtonian flow and for a Bingham plastic the friction factor is given by:

$$C_f = (16/Re)(S/8c)$$

where c is the ratio of the yield value to the shearing stress at the pipe wall and S is the plasticity number. For pseudoplastic and dilatant fluids for which the power law relation holds the friction factor is given by:

$$C_f = \frac{16}{Re}\left(\frac{3n+1}{4n}\right)$$

whereupon C_f is then plotted over a range of Reynolds numbers for various values of S and n.

This approach by Weltmann is based on the assumption that the fluid is an ideal Bingham plastic or true power law fluid and is therefore not as applicable as the method of Metzner and Reed.

The various methods for predicting pressure losses and flow rates of non-Newtonian systems published to date involve various degrees of theoretical rigour, computational ease and accuracy of results. The method of Metzner and Reed is theoretically rigourous for all time independent fluids including Bingham plastics but involves detailed computations. Additionally, the fact that it is difficult to reproduce results for non-Newtonian systems consistently makes it hard to know just exactly how well the predictive models agree with experimental results.

1.5 Turbulent Flow of Time-Independent Fluids in Pipes

Little work has been done to predict the onset of turbulence or quantify the subsequent flow characteristics of non-Newtonian fluids in circular pipes. Many of the early investigators took an empirical approach to the study of turbulence and in general it was viewed that at high enough Reynolds numbers the apparent viscosity of the system remained fairly constant due to the high shear rates which suppressed non-Newtonian behaviour. Subsequently it was felt that the conventional Newtonian friction factor diagram sufficed to describe non-Newtonian flows in the turbulent region provided the viscosity used in the Reynolds number was chosen judiciously.

Caldwell and Babbitt (1941) developed equations for lower and upper critical velocities at which turbulence began and used the viscosity of the dispersion medium of the sludge under study to determine a turbulent Re. The friction factor corresponding to Re is the same as if a true fluid such as water were the flowing material. What they failed to realize however was the unlikely chance that the limiting viscosity would be as low as that of the dispersion medium.

Winding et al. (1947) and Alves et al. (1952) suggested that the limiting viscosity at infinite shear rate μ_∞, is a more appropriate value to substitute into Re and obtained fairly successful correlations for non-Newtonians

with the Newtonian C_f curve in the turbulent region. Winding et al. suggest that laminar to turbulent transition in pipes occurs when the Reynolds number based on the viscosity at zero shear rate μ_o, reaches 2100. Alves et al. define turbulence as commencing when $Re = \rho u_m D/\mu_\infty$ reaches 2100 since the viscosity at zero shear rate will not be meaningful at higher shears where turbulence sets in.

Hedstrom (1952) proposed that the onset of turbulence occurs when the laminar friction factor curve (a function of He) intersects the turbulent friction curve for Newtonian fluids.

Weltmann's (1956) work with Bingham plastics suggests essentially the same criterion as that of Hedstrom; namely that the Reynolds number ($\rho u_m D/\mu_p$) given by the intersection of the line in the laminar region for the particular fluid in question and the turbulent friction line for Newtonians is the Re value at which turbulence begins.

Metzner and Reed (1955) extended the concept of a generalized Reynolds number into the turbulent region thus avoiding the assumption of constant viscosity. They proposed a criterion for the onset of turbulence based on the friction factor and suggested that the transition from laminar to turbulent flow in pipes occurred when C_f fell below 0.008 on their generalized C_f diagram.

A theoretical approach to the problem of correlating turbulent friction factors for smooth pipes was taken by

Dodge and Metzner (1959). The final resistance law correlation they developed represents a generalization of von Karman's equation for Newtonian fluids in turbulent flow and is applicable to all time independent non-Newtonians irrespective of rheological classification.

By applying standard methods of dimensional analysis to equation (1.19) describing a power law fluid, they showed that:

$$C_f = f(Re^o, n)$$

where Re^o has the form of a Reynolds number. They next proceeded to calculate the form of this functional relationship and came up with an equation of similar form to the von Karman equation for turbulent Newtonian systems:

$$\frac{1}{\sqrt{C_f}} = R\log\left[Re^o(C_f)^{1-n/2}\right]+G \qquad (1.22)$$

where R is a coefficient, G a constant to be determined and:

$$Re^o = D^n u_m^{2-n}\rho/k$$

Re^o however is not so convenient a Reynolds number for correlation purposes as the one proposed by Metzner and Reed (1955) since it does not result in a unique relationship between C_f and Re in the laminar flow region. The generalized Reynolds number Re', does result in a unique relationship in the laminar region for all values of n, namely the familiar relationship $C_f = 16/Re'$.

It can be shown that for power law fluids Re^{o} and Re' are related as follows:

$$Re^{o} = 1/8(6n'+2/n')^{n'}Re'$$

where k', n' and Re' are as defined previously.

Introduction of Re' in place of Re^{o} in (1.22) yields:

$$\frac{1}{\sqrt{C_f}} = R\log\left[Re'(C_f)^{1-n'/2}\right]+G' \qquad (1.23)$$

where $G' = R\log\left[(1/8)(6n'+2/n')^{n'}\right]+G$

If equation (1.23) is valid as postulated, it should hold for the Newtonian case where n' is unity. For this case, the equation reduces to:

$$\frac{1}{\sqrt{C_f}} = R\log\left[\frac{Du_m\rho\sqrt{C_f}}{\mu}\right]+G'$$

Newtonian data agreed very well with such a relationship and led to the von Karman formula:

$$\frac{1}{\sqrt{C_f}} = 4.0\log\left[\frac{Du_m\rho\sqrt{C_f}}{\mu}\right]-0.40 \qquad (1.24)$$

Equation (1.23) is the form of the equation relating the friction factor and Reynolds number for the turbulent flow of a power law fluid in a smooth pipe. It remains for R and G' in the case of a power law fluid to be determined experimentally as functions of n'. To find R, $1/\sqrt{C_f}$ is plotted against $Re'(C_f)^{1-n'/2}$. The slope of this plot as seen from (1.23) gives R.

This procedure was carried out for a range of pipe sizes for fluids of various flow indices n' to give values of Re as a function of n'. Theoretical considerations suggest that these results would be correlated by plotting R against n' logarithmically. When this was done by fitting a line through the data using the method of least squares, the equation of the line was found to be:

$$R = 4.0/(n')^{0.75} \tag{1.25}$$

and the condition that R = 4.0 when n' = 1 was satisfied. This function, besides fitting the data, satisfies the theoretical restrictions imposed upon it.

The function G' is determined by substituting R values given by (1.25) into equation (1.23) and plotting -G' against n' logarithmically. A straight line fitted through this data yielded the equation:

$$G' = -0.40/(n')^{1.2} \tag{1.26}$$

This satisfies the Newtonian condition of G' = -0.40 when n' = 1. The final proposed friction factor correlation is obtained by substituting for R and G' in (1.23). This yields the general form of the von Karman equation given in (1.24):

$$\frac{1}{\sqrt{C_f}} = \frac{4.0}{(n')^{0.75}} \log\left[Re'(C_f)^{1-n'/2} \right] - \frac{0.40}{(n')^{1.2}} \tag{1.27}$$

Although the above analysis is based strictly upon

the power law model of fluid flow, equation (1.27) can be used successfully with non power law fluids, provided that the fluid property parameters (n' and k') are evaluated at the wall shear stress. Excellent agreement was found beween predicted and experimental friction factors when this was done.

In general, the non-Newtonian friction curve in turbulent flow agrees quite well with the Newtonian curve and the latter can be used quite successfully for most design purposes. This is because most non-Newtonian systems appear to behave as Newtonians at higher shear rates where the structure is completely broken down. If increased accuracy is required in determining C_f, the method of Dodge and Metzner gives excellent results although the computations are again tedious.

1.6 Time-Dependent Non-Newtonian Fluids - Thixotropy

A thixotropic fluid (rheopectic fluids are rare and therefore will not be discussed) has a yield stress and viscosity which significantly decrease both reversibly and isothermally with a distinct time dependence on the application of shear strain. Strictly speaking, thixotropic fluids which show evidence of a yield stress are often termed 'false bodies'. This distinction is made to separate true thixotropic materials which break down completely with high shear stresses, from materials (notably Bingham plastics which show thixotropic behaviour) which do not lose their

solid properties entirely and still exhibit a yield value although it may be diminished (Wilkinson, 1960). Goodeve (1939) contends that a complete transformation from a gel to a sol is not a prerequisite for thixotropy. A yield value may still be evident but the material does become less elastic; a partial transformation is all that is necessary.

The term thixotropy was originally used to characterize colloidal suspensions of irregular particle shape which underwent isothermal gel-sol-gel transformations. These suspensions had sufficient rigidity to support their own weight when suspended in an inverted test tube, exhibiting a yield stress for no flow. When the suspension was vigourously shaken, its structure transformed to that of a freely flowing liquid with viscosity the order of the dispersing fluid. After a sufficient period of rest the structure reverted back to its original gel form.

As an example of thixotropic behaviour consider a material confined in a co-axial cylinder rotational viscometer. After the material has been rested for a sufficient time to allow complete structural buildup to take place, one of the cylinders is rotated at constant speed. The torque indicated at the other cylinder would then decrease with time as shown in Fig. 1.4. The rate of decrease and the final torque both depend on the speed.

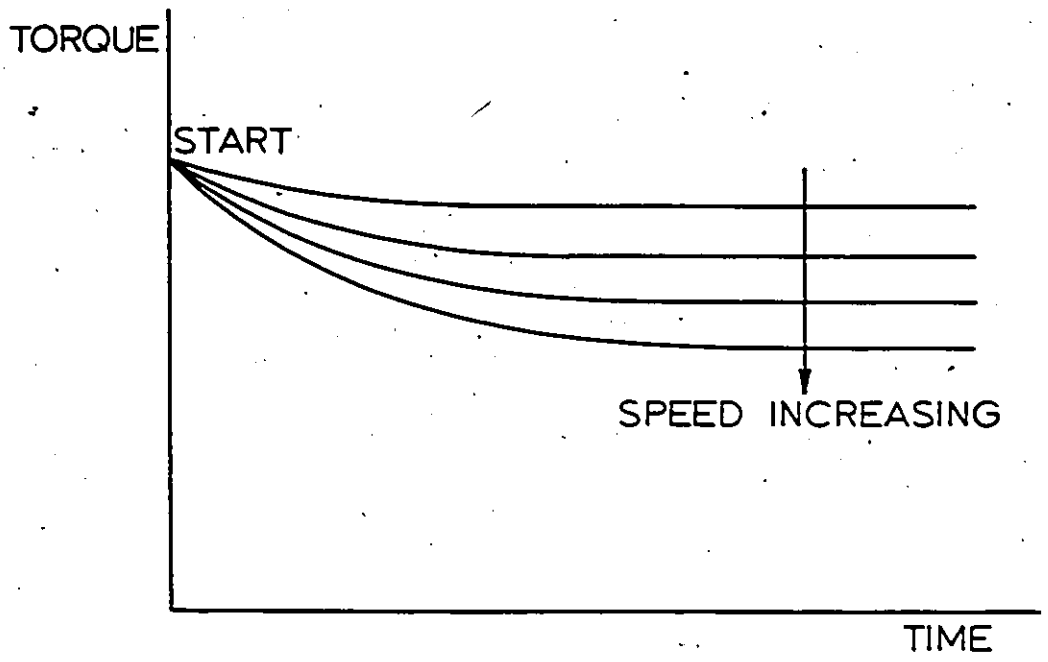

Figure 1.4 Thixotropic behaviour as a function of time

Similarly, thixotropic breakdown can be shown in a capillary tube viscometer by plotting $a\Delta P/2L$ against $q/\pi a^3$ (Fig. 1.5).

The unique plot which was obtained for a time-independent material now becomes a series of curves which vary depending on the diameter and length of the tube. Since increased thixotropic breakdown occurs at prolonged and higher rates of shear, it is more pronounced in longer pipes of smaller diameter. For this reason, quantitative analysis of thixotropic systems are usually made in rotational instruments for which there are precise and uniform rates of shear.

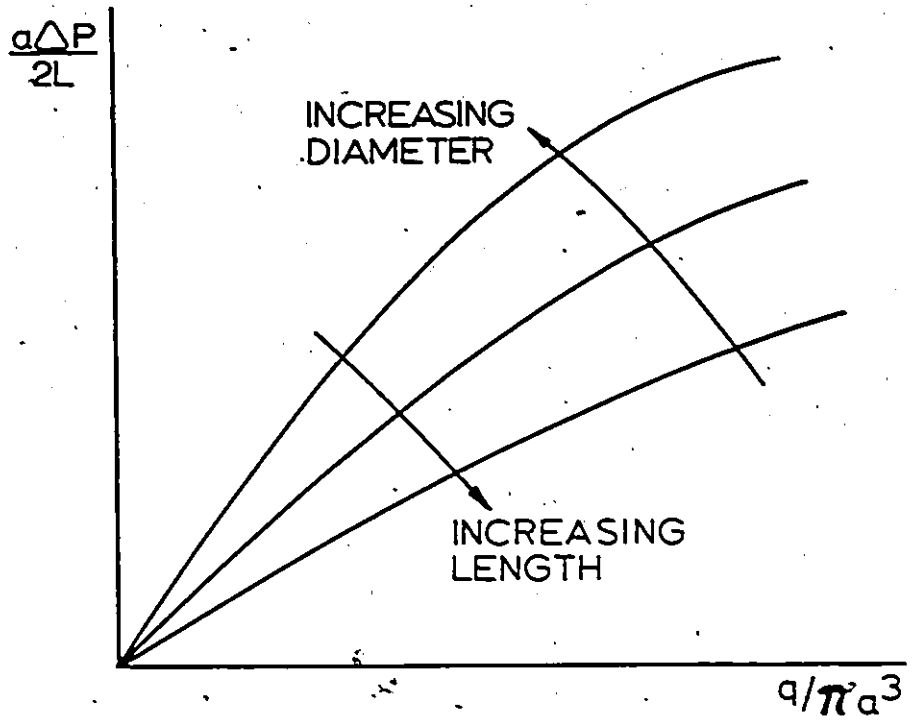

Figure 1.5 Thixotropic behaviour in a capillary tube viscometer

Goodeve and Whitfield (1908) proposed a quantitative theory of viscosity in which the magnitude of thixotropy was expressed by a single quantity called 'the coefficient of thixotropy', defined as the limiting slope of the viscosity-reciprocal shear rate curve as $\dot{\gamma}$ approaches a high value. Green and Weltmann (1944) feel that it is impossible to measure thixotropy from a single consistency curve in this manner and go about studying the hysteresis loop formed as a thixotropic substance is sheared at various increasing and then decreasing rates of shear in a rotational instrument. They argue that to learn something of the extent and nature of thixotropic change in breakdown or buildup, it is

necessary to have data that cover the before and after states (Green and Weltmann, 1943).

As the 'upcurve' (curve OA in Fig. 1.6) is formed, the material breaks down under the increased $\dot{\gamma}$. Once a maximum $\dot{\gamma}$ is attained a 'downcurve' may be started immediately (line AO) resulting in a rather small loop or $\dot{\gamma}$ may be maintained until the material breaks down to an equilibrium value of shear stress and then the downcurve is commenced, resulting in the largest possible hysteresis loop (OACO). Regardless of where the downcurve is commenced (A, B or C), it was always found to be linear and to pass roughly through the same yield point. The area of the hysteresis loop was used to indicate the degree of thixotropy as it depends on the rates of increase and decrease of $\dot{\gamma}$. If the rate of $\dot{\gamma}$ throughout a cycle is such that equilibrium is always obtained between the breakdown and buildup of the structure, a single curve is obtained (curve OAO). This case represents plasticity with no degree of thixotropy evident.

From work on thixotropic materials of the Bingham plastic type, Weltmann (1943) has developed the following relationship:

$$\exp\left[-(\mu_1-\mu_2)/J\right] = t_1/t_2$$

where μ_1 and μ_2 are plastic viscosities determined at two times of shear duration, t_1 and t_2. Plastic viscosity is used as opposed to apparent viscosity because in non-thixo-

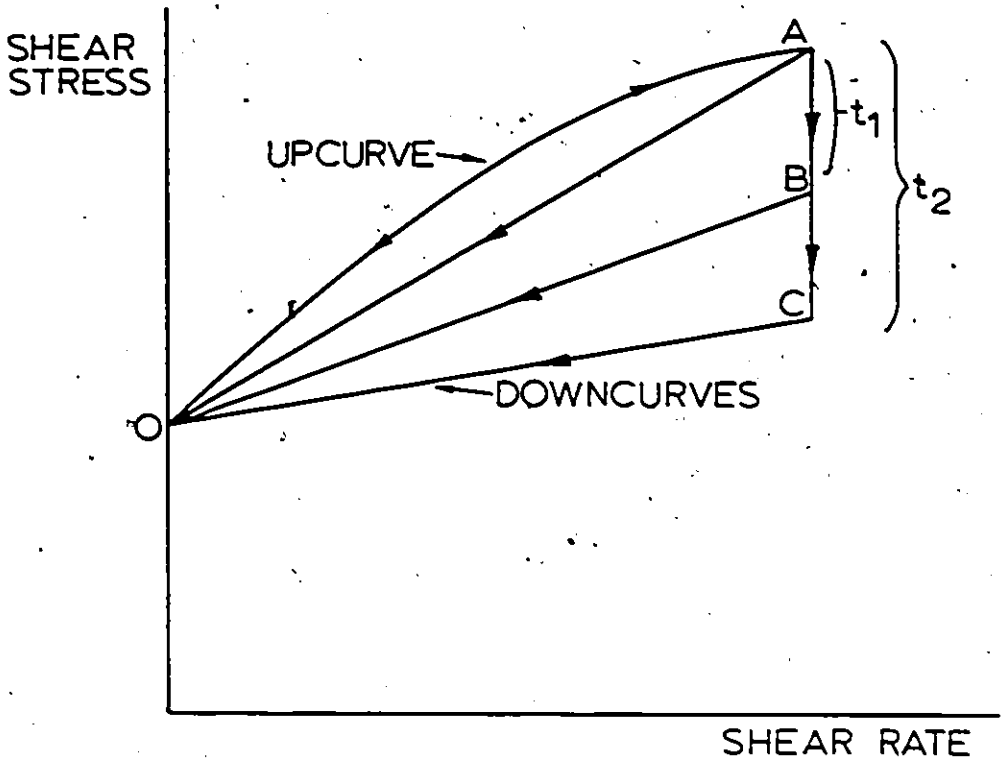

Figure 1.6 Thixotropic hysteresis loops

tropic plastics it is a constant, being independent of shear rate (μ_p for a true Bingham plastic). In thixotropic materials, the plastic viscosity decreases with agitation. J is the product of rate of breakdown of plastic viscosity and time, that is, the time during which the agitation at constant rate of shear has been applied called the 'time coefficient of thixotropic breakdown'.

$$J = (\mu_1-\mu_2)/\ln(t_2/t_1)$$

J is independent of the instrument and has the same dimensions as viscosity.

An analysis of the hysteresis loop (Green and Weltmann, 1944, 1946) also gave two coefficients M and V of

thixotropic breakdown. M is the loss in shearing force per unit area per unit increase in velocity gradient. V gives the change in yield value per unit change in plastic viscosity.

$$M = 2(\mu_1-\mu_2)/\ln(\omega_2^2/\omega_1^2)$$

$$V = (\tau_2-\tau_1)/(\mu_1-\mu_2)$$

Other studies of thixotropic materials using the hysteresis loop method include that of Gabrysh et al. (1961) who studied a colloidal suspension of thixotropic attapulgite clay in water and Leonard and Hazlett (1966) who investigated flow behaviour of aqueous magnesium montmorillonite suspensions.

Unfortunately, the use of hysteresis loops to describe thixotropic systems is rather limited (Bauer and Collins, 1967) since:

1. They are qualitative and depend on the degree of equilibrium reached. Thus unless equilibrium is attained the results have little value; as in the case of transient flows, e.g., flow through short pipes, valves or fittings.
2. They are difficult to interpret when the rebuilding of a structure from equilibrium is extremely fast.

Interpretation of these loops is of little quantitative value, because the loop cannot separate the different

factors involved in thixotropic change i.e., rates of change, amounts of change, and changes in response at different shear rates and with different past histories. The hysteresis loop method says little about the structure except that it is changing (Joye and Poehlein, 1971).

Although various mechanisms for thixotropic behaviour have been postulated none are definitively accepted. It is generally accepted that thixotropic materials at rest have an internal structure which may arise due to attractive forces at points on anisometric dispersed particles. The attractive forces between particles were found to be electrostatic. To show this, an electric field was applied parallel to the axis of a rotational viscometer containing an aqueous bentonite solution. When the field was switched off, the torque on the instrument decreased (Schultz-Grunow, 1962). The flow properties of a thixotropic substance were thought to be governed by two effects acting adversely. On one hand attractive forces acting between the suspended particles generate clusters and on the other hand the clusters are collapsing by the action of shear forces. When a shear force is applied, breaking of the bonds which form the network occurs since the kinetic energy of the system increases due to the forward flow, and consequently the particles take up random orientation. Upon continued shear, if the solution is sufficiently dilute, it may act as virtually a Newtonian liquid with properties determined by the sus-

pending medium. On deletion of the shearing, random Brownian motion within the stationary fluid allows attractive sites on different particles to adhere and form new linkages and eventually re-establish the original network (Joye and Poehlein, 1971).

Hahn, Ree and Eyring (1959) proposed a quantitative theory of thixotropy which predicts the viscosities of thixotropic polymers and hydrocarbons under working conditions. They assume that in a flow system of thixotropic substances (such as grease) there exist two kinds of molecules, extended entangled and coiled disentangled, the former non-Newtonian in their flow nature and the latter Newtonian. The relative amounts of the entangled and disentangled molecules as determined by the equilibrium constant for entangled $\rightleftharpoons$ disentangled states characterizes the degree of thixotropy.

Fredrickson (1970) presents a model for the rheological behaviour of thixotropic systems exhibiting no elastic or anisotropic effects. The model is advanced for suspensions of rigid, solid particles in liquids (such as clay suspensions) and is not expected to be valid for materials of polymeric constitution or for suspensions of elastic deformable particles in liquids.

Few attempts have been made to quantify the flow of thixotropic materials in pipe lines since in most cases they can be treated as time independent because they are broken down by the high shear rates involved. It is also

somewhat difficult to define the concentration at which a pronounced yield stress occurs. This makes it somewhat awkward to design pipe line systems for thixotropic slurries.

In 1965, Cheng, Ray and Valentin published results on the pumping of bentonite suspensions through pipes and pipe fittings. They presented data for concentrations of 1.7%, 4.8% and 7.8% and observed that for equilibrium conditions the shear stress data obtained for laminar flow in small bore tubes agreed with that from laboratory viscometers and thus deduced that equilibrium curves can be determined using laboratory viscometers. They also determined that thixotropic behaviour became more pronounced at higher concentrations and that yield values increased significantly with concentration.

Most work on thixotropic systems has been aimed at quantifying the degree to which thixotropy exists and to establishing a rheological mechanism of thixotropy. This has been done primarily in concentric cylinder viscometers and few correlations with pipe line systems have been attempted since the material is usually pumped in its equilibrium state. Methods such as the analysis of hysteresis loops are of little value for the designer of thixotropic systems. Studies such as those of Cheng et al. have shown that the substances become more thixotopic as the slurry concentration in pipe line flows is increased, but a general rheological model for time dependent fluids has not yet been postulated.

1.7 Scope of the Present Work

The purpose of this work was to study the pipe line flow of non-Newtonian fluids. Specifically, data are obtained for aqueous bentonite slurries having concentrations of 1.96%, 4.0%, 5.0%, 6.0% and 8.0% by weight which have been pumped in a small scale pipe line. Pressure drops were recorded for various flow rates of the suspensions through three glass test sections of different diameters. Three test sections are used so that experimental data taken from any one may be used to predict flow conditions in the second or third and subsequently compared for accuracy with results in these other tubes. Secondly, thixotropic effects can be detected in test sections of different length and diameter.

The pipe line system was originally designed solely for the study of the laminar flow of these fluids, but the experiments have been carried over into the turbulent region. Data are presented in the form of shear diagrams for all concentrations studied. The shear diagram is the rheological thumbprint of any fluid and is the basis for subsequent analysis in the form of friction factor diagrams. Power consumption in pumping the various concentrations of slurries were calculated from pressure drop measurements per unit length of pipe.

In an age where energy is becoming an expensive and ever diminishing commodity, it is necessary to continue the

study of non-Newtonian flow in pipes so that the most economical design procedures can be established.

CHAPTER 2

DESIGN AND DESCRIPTION OF EXPERIMENTAL APPARATUS

2.1 General

The design of the model pipe line built to study the flow of non-Newtonian suspensions was based on the viscosity and flow rates of aqueous glycerol solutions, a Newtonian fluid. Three nominal diameters for the test sections were chosen and the pressure drop per unit length of the three pipes were determined using the Hagen-Poiseuille equation. The viscosity range of interest for the studies was to have been between 0.001 and 0.1 Pa·s (or 1 and 100 centipoise) so that several convenient viscosities of aqueous glycerol within this range have been chosen for design calculations (Appendix B). Since the work was originally intended to encompass only laminar flows, a minimum Reynolds number of 1000 and maximum of 2000 were employed in the calculations.

Once approximate pressure drops per unit length of pipe were determined, the test section lengths were approximated depending upon the range and sensitivity of the pressure measuring device which in this case was a liquid 'U' tube manometer or a differential pressure transducer. Entrance lengths were then estimated so that overall test section lengths can be determined.

Appendix B gives a detailed description of the pro-

cedure used to determine test section configurations.

2.2 Description of the Flow Loop

A schematic diagram of the apparatus is given in Fig. 2.1. The fluid or suspension to be pumped was generally premixed at a separate location and then added to the main circulating tank constructed from a 22.5 liter drum. The circulating tank was supported by a 3.8 cm inlet pipe which fed the mixture directly to the pump inlet. A small gate valve affixed to the bottom of the circulating tank was used to drain the system. The pump was a progressing cavity Moyno type FA-56, which has a capacity of 4 liters per second and a maximum output pressure of 0.17 MPa. The pump was directly coupled to a 1.12 kW variable speed D.C. motor. The motor and pump were mounted firmly on a supporting base made from welded angle iron stock. A short flexible hose connects the pump outlet to the remainder of the delivery system so that any inherent pump noise was partially damped from the system. A 9 L capacity surge tank situated in the delivery tube just after the pump was found to be of significant importance in damping out oscillatory fluid motions in the test section of the apparatus.

A 2.54 cm diameter glass pipe approximately 3 m long connected the pump to the test section. Two bellows type couplings joined the removable test section to the remainder of the loop. The test section was supported independently from the remainder of the system and the bellows connectors

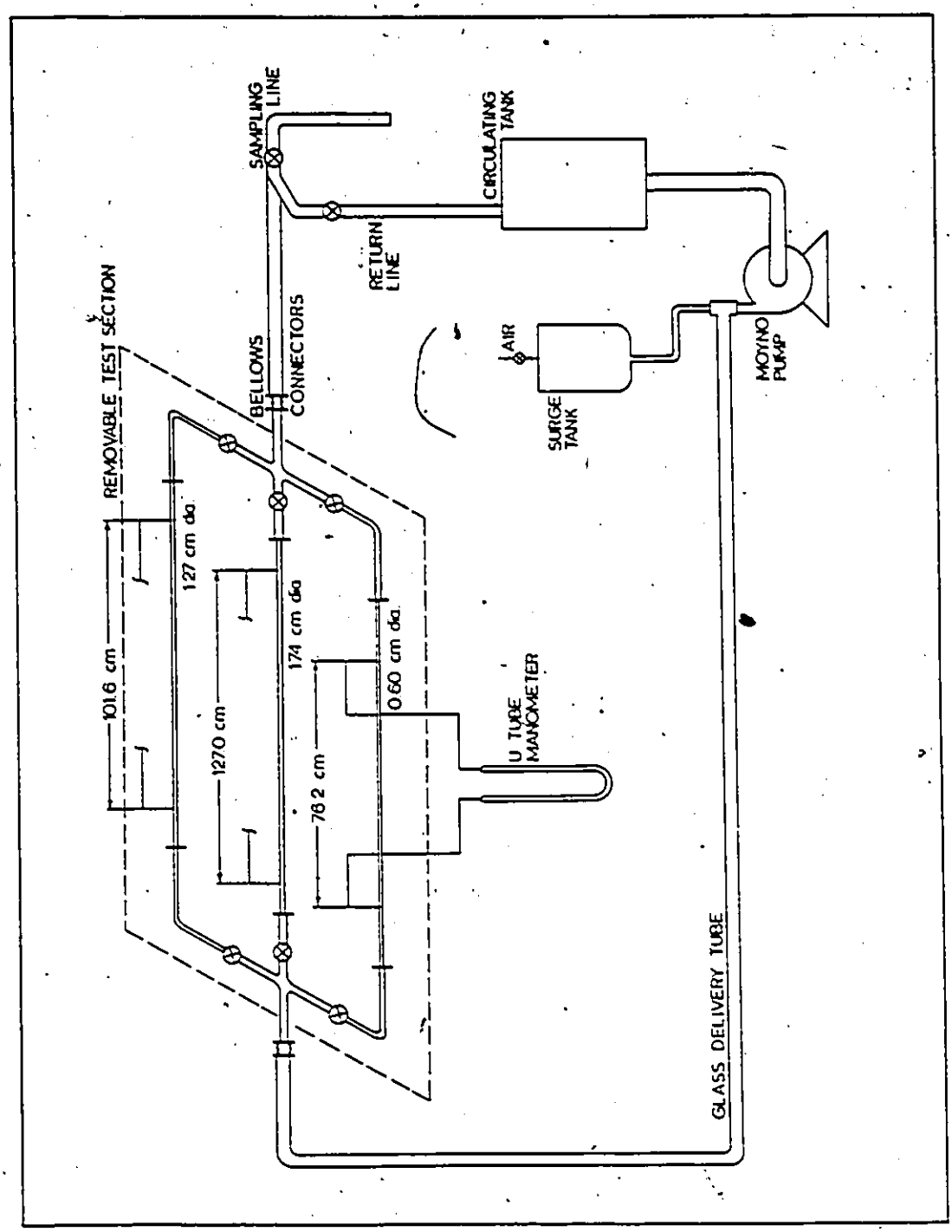

Figure 2.1 Schematic of experimental apparatus

damped out any vibration from the delivery or discharge sections. The discharge section consisted entirely of 2.54 cm copper tube and fittings and was divided into two branches. The first branch returned the flow directly to the circulating tank and the second was a sampling line which was used to collect a volume of the fluid over a known time interval to determine the flow rate. A flexible hose connected to the sampling line diverted the flow to the sampling jar and back to the circulating tank after the sample was taken.

The entire loop was supported by four angle iron brackets bolted securely to the floor. Wooden split bearings supported the pipe at four different locations on two of these brackets. The test section as mentioned, was supported independently from underneath by the other two brackets.

2.3 Description of the Test Section

The removable test section was mounted independently from the remainder of the flow loop to help isolate it from pump noise and external vibrations. It was built upon a 1.9 cm plywood substrate approximately 2.5 m long and 0.6 m in width which in turn was bolted to two angle iron supporting members. The piping network was held firmly onto the plywood by wooden split bearings. In this way the glass test sections need not be supported independently along their lengths.

The flow entered the test section from the bellows coupling and was directed into a three-way manifold system.

The manifold was constructed of copper pipe and brass fittings because of its low cost, simplicity of construction and ruggedness. Directly opposite to the inlet, the 2.54 cm network reduced down and flanged to the 1.74 cm diameter glass test section. On either side of the inlet, the flow network was reduced down and directed to either the 1.27 cm or 0.60 cm glass test section. An approximate entrance length (Appendix B) allowed the flow profile to develop before it reached the glass tubes.

The copper manifold was connected to the three glass test sections by way of quick fit connector flanges which bolted to a steel flange soldered to the manifold. The glass sections were bolted down appropriately to stop leaks after the system was operating. The pipe manifold at the discharge end of the test section was exactly the same as the one at the inlet. A sufficient number of gate valves were included in the system to direct flow through the desired test section.

2.4 Description of the Glass Sections

The three glass test sections were fitted between their respective manifold flanges and held secure using quick fit connectors. The 1.74 cm test section was purchased as a standard 1.52 m pipe length and had only to be pressure tapped. The 1.27 and 0.60 cm sections were made up completely by the glass blower. Glass tubing of fairly solid wall thickness was molded right into the test sections for pressure taps. Tygon tubing of 0.63 cm I.D. was slipped over

these pressure taps to act as pressure transmission lines and easily held in place with small hose clamps. The pressure taps were molded smoothly into the test sections so that no protrusion was left to cause any disturbance to the flow.

The test sections which were manufactured completely by the glass blower had a slight warpage in them due to heating when the quick fit ends were molded on and due to the fact that the ends could not be molded on perfectly square with the tubes. Hence when the sections were bolted between the manifolds, the flanges had to be tightened carefully and such that as little bowing as possible occurred in the sections. This warpage did not cause any out of roundness or change of internal diameter in the test section, but the sections had to be torqued down carefully to ensure that they were straight. A small spirit level was used to align them horizontally.

2.5 Determination of Test Section Diameters

The mean internal diameter of each test section was determined prior to having them pressure tapped by filling each tube with a known volume (weight) of mercury and then measuring the height of the Hg column in each tube. The diameter is easily calculated from the equation for the volume of a right circular cylinder (see Appendix C).

CHAPTER 3

EXPERIMENTAL PROCEDURE AND ANALYSIS OF DATA

3.1 Procedure

The fluid to be tested in the model pipe line was prepared in sufficient quantity before being poured into the circulating tank. For the Newtonian tests a blend of equal amounts of kerosene and 10W40 motor oil was used (section 4.1).

For the non-Newtonian tests five clay slurries were produced by accurately weighing out the required amount of tap water and bentonite powder to achieve the desired concentration (see Table E.1 of Appendix E). The bentonite powder was then premixed with enough methanol to disperse it into a highly concentrated slurry which was then carefully poured into the container of water while stirring vigourously. This prevented the clay powder from flocculating in the water, facilitating preparation of the mixture. The suspension was allowed to settle over night while it reached room temperature. The residual water-methanol mixture of the low concentration slurries which did settle was syphoned off of the top and replaced by an equivalent amount of fresh water. The mixture was stirred well before being introduced into the system which had been previously cleaned and drained.

The fluid in the pipe line system was pumped around at an intermediate flow rate prior to testing to establish thermal equilibrium and allow air bubbles to dissipate out.

Meanwhile, the manometer was carefully placed into the system across the pressure taps of the desired test section and the tygon lines were filled with the pressure transmitting fluid. The appropriate test sections were then closed off and the flow rate was adjusted for the first test in the remaining tube. Sufficient time was allowed for the flow to stabilize before pressure drops and flow rates were recorded for each test.

The manometer fluid was either mercury or carbon tetrachloride depending on the pressure range. Kerosene was used as the pressure transmitting fluid for the Newtonian mixture and water was used for all of the slurry tests. Initially a dynamically responsive differential pressure transducer was used to indicate that the flow instabilities were minimal, but was not used for the majority of the experiments because of the lack of precision.

The Newtonian data are given in Tables D.1 to D.3 of Appendix D and the bentonite data are summarized in the data sheets of Appendix E. All tests were repeated at least twice to ensure good agreement between the actual flow rates and each slurry concentration was mixed and tested at least twice as a check on results although complete data are not listed. It was found that agreement between the separate experiments was quite good.

A flow rate was determined, the pressure drop was read directly from the differential 'U' manometer and the temperature of the sample was recorded in ^{o}C. Average values of q, ΔP and

θ were computed from two samples for each test. A sufficient sample of the fluid was retained after testing to determine the density of the mixture and stored for any additional tests.

3.2 Analysis of Data

In order to interpret the pipe line data, it had to be converted to the consistency variables $a\Delta P/2L$ and $4q/\pi a^3$ so that a shear diagram could be plotted. The first step was to correct the differential pressure term ΔP, by subtracting the equivalent head of the transmitting fluid from the differential reading of the manometer fluid which was recorded. As the transmitting fluid was either water (specific gravity = 1.00) or kerosene (s.g. = 0.82), the equivalent head would be the product of differential manometer reading and specific weight of the transmitting fluid. This was then converted to either cm Hg (s.g. = 13.60) or cm CCl_4 (s.g. = 1.59) and subtracted from the original differential reading. The corrected pressure in kPa was then divided by the appropriate length between the pressure taps to yield a pressure drop per unit tube length ($\Delta P/L$) which when multiplied by a/2 gives the shear stress at the wall. The corresponding shear rate is found by substituting q_{avg} from the data sheets into the equation $\dot{\gamma} = 4q/\pi a^3$. The shear diagram is a smooth curve which best fits all of the data points. The results are shown in Figs. 4.1 and 4.3 to 4.7 of Chapter 4.

The correlation of the data consisted of plotting friction factor diagrams for each fluid for comparison with

the standard Newtonian friction curves. Plotting the friction factor diagram for the Newtonian oil was straight forward and is outlined in section 4.1. The slurry analysis consisted of first obtaining values of τ_w for various values of $\dot{\gamma}$ over its range from the shear diagram. This was done rather than using the original data due to the smoothing effect of the curve. An apparent viscosity for flow in the 0.60 cm diameter tube was computed by dividing τ_w by $\dot{\gamma}$. The Fanning friction factor was calculated in the usual mannner, i.e.,

$$C_f = \frac{a\Delta P}{2L} \Big/ \frac{1}{2}\rho u_m^2$$

The mean velocity was found by interpolating the flow rate for each chosen shear rate from a plot of q_{avg} vs. $\dot{\gamma}$ for the original data and dividing by the cross sectional area of the tube.

The Reynolds number was calculated in all three tubes by using the apparent viscosity, μ_a from the 0.60 cm diameter tube.

Finally, the power requirement per unit length of tube to pump the fluid was determined by multiplying the flow rate and pressure drop and dividing by the length of tube over which ΔP was measured.

A discussion of the experimental errors can be found in Appendix H.

CHAPTER 4

EXPERIMENTAL PIPE LINE RESULTS

4.1 Newtonian Results

In order to determine how well the experimental equipment functioned and how accurately it could be used, a series of tests were done on a Newtonian oil solution prior to testing the non-Newtonian slurries. It was decided to run a series of tests on a mixture composed of equal amounts of kerosene and SAE 10W40 motor oil (denoted as 50/50 kerosene in 10W40). Such a blend yielded a fluid whose consistency would be comparable to that of the non-Newtonian slurries to be tested. The pipe line system was cleaned with a soap solution and rinsed of all debris prior to running the tests. A sufficient quantity of 50/50 kerosene in 10W40 was introduced into the system and data were taken as outlined in Chapter 3. The results of the experiment on this fluid are tabulated in Appendix D.

The analysis of the data consisted of plotting the shear diagram in terms of the consistency variables. The shear stress and shear rate calculations are tabulated in Tables D.4 to D.6. Kerosene was used as the pressure transmitting fluid in conjunction with the mercury manometer.

The plot of shear stress against shear rate yielded a linear relationship of approximately the same slope for all three test sections (Fig. 4.1).

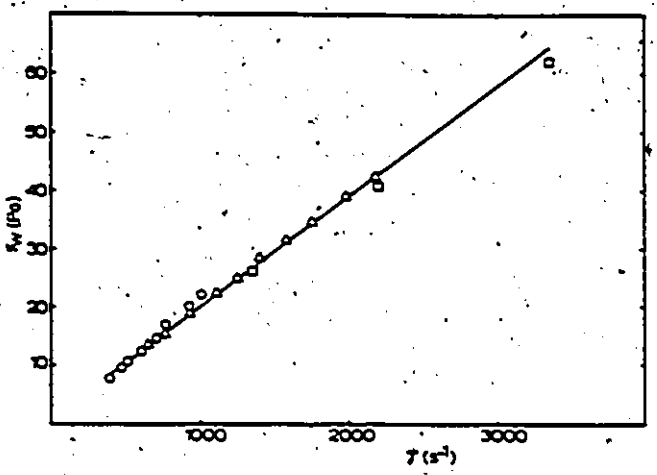

Figure 4.1 Wall shear stress vs. apparent shear rate for 50/50 kerosene in 10W40
□0.60 cm diameter tube
△1.27 cm diameter tube
○1.74 cm diameter tube

This was very encouraging as the linear shear diagram indicated that the flow was Newtonian over the entire shear rate range as would be expected and the viscosity is therefore constant for all Reynolds numbers.

A value of viscosity was obtained for each of the three tubes by calculating the slope of the shear diagram. The results are summarized in Table 4.1.

A sample of the fluid was then retrieved from the pipe line system and its viscosity was determined in a Brookfield cone and plate viscometer at temperatures close to those of the pipe line results. The comparison of viscosities is made in Table 4.1. The agreement between viscosities obtained by the two methods is quite good. A second sample of the fluid

Table 4.1 Newtonian oil viscosities

Tube Diameter (cm)	Absolute Viscosity (Pa·s)		Average Temp. (°C)
	Pipe line	Brookfield	
0.60	0.018	0.0201	21.5 21.6
1.27	0.020	0.0204	20.8 21.0
1.74	0.021	0.0198	21.9 22.0

was retained and its density was found to be 0.84 g/cm^3.

To complete the analysis of the Newtonian fluid, a friction factor-Reynolds number diagram was plotted (Fig. 4.2). The Reynolds number for each tube was computed using the value of viscosity obtained for that tube from the shear diagram (Table 4.1). The computations are shown in Tables D.7 to D.9 of Appendix D.

The data from all three tubes fit the curve $C_f = 16/Re$ quite well indicating that the system yields substantial results for Newtonian fluids of fairly low viscosity. Since development lengths are usually shorter for non-Newtonian fluids, it can be postulated that non-Newtonian data gathered from the same system in the same manner should be an accurate representation of the flow conditions. Turbulent flow of the Newtonian fluid was not studied.

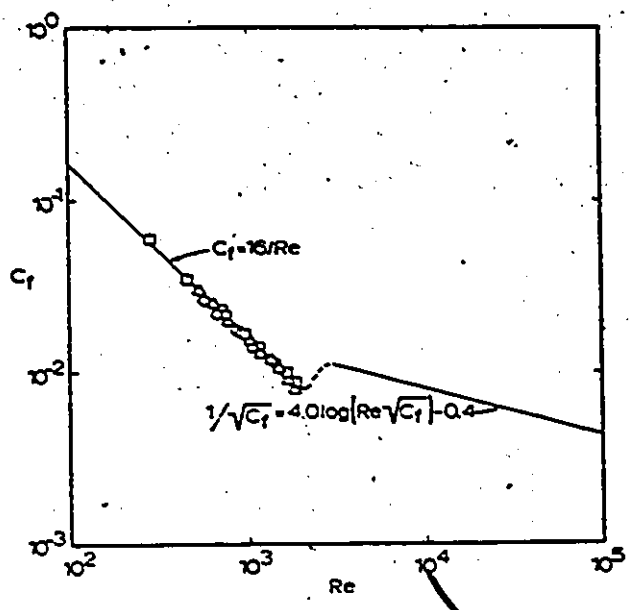

Figure 4.2 Friction factor vs. Reynolds number for
50/50 kerosene in 10W40
□ 0.60 cm diameter tube
△ 1.27 cm diameter tube
○ 1.74 cm diameter tube

4.2 Bentonite Slurry Results

Five different slurry concentrations ranging from 1.96% by weight to 8.0% by weight were tested. The composition of the slurries is given in Table E.1 along with the density of the mixture at roughly the temperature at which it was tested. The experimental pipe line results are given in Tables E.2 to E.16 of Appendix E.

In the first instance, shear diagrams were plotted for each bentonite concentration (Figs. 4.3 to 4.7) in terms of the consistency variables $a\Delta P/2L$ and $4q/\pi a^3$. The shear stress-shear rate calculations are outlined in Chapter 3 and

are summarized in Tables E.17 to E.31. Not all the data points are included on the shear diagrams for the 0.60 cm diameter tube because the shear rates get much higher than in the other tubes. The general trend of the curve does not change abruptly however.

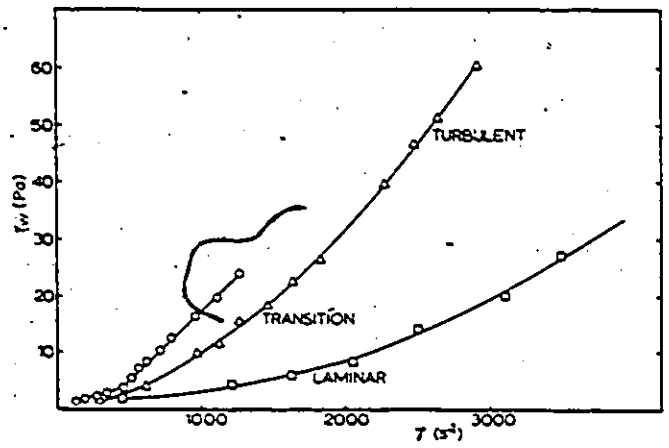

Figure 4.3 Wall shear stress vs. apparent shear rate for 1.96% suspension
□0.60 cm diameter tube
△1.27 cm diameter tube
○1.74 cm diameter tube

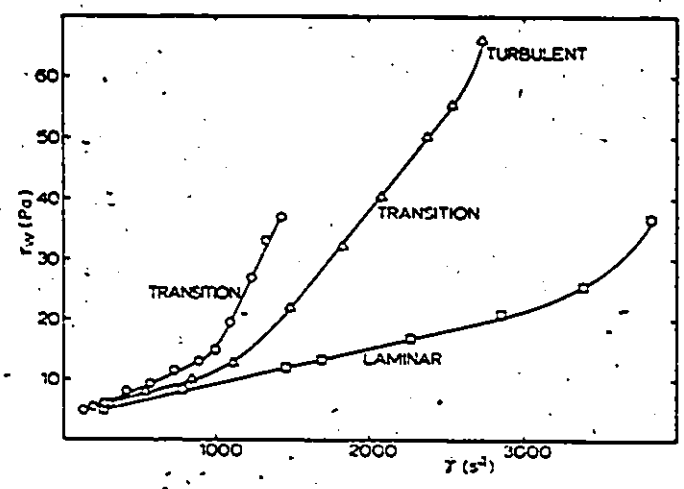

Figure 4.4 Wall shear stress vs. apparent shear rate for 4.0% suspension
□0.60 cm diameter tube
△1.27 cm diameter tube
○1.74 cm diameter tube

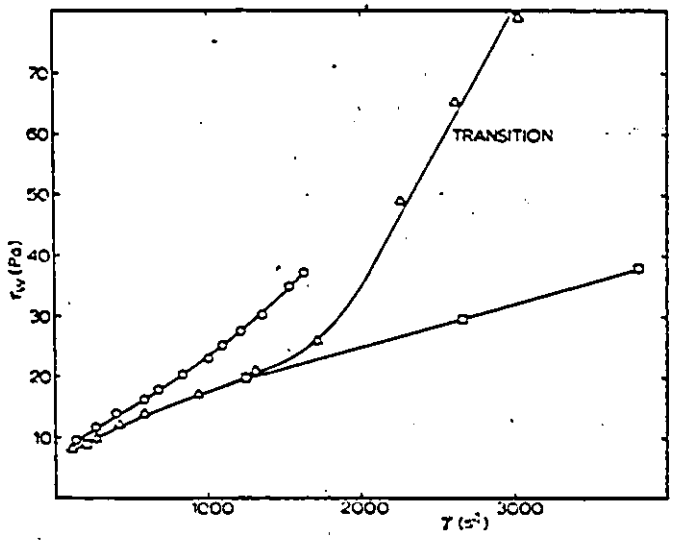

Figure 4.5 Wall shear stress vs. apparent shear rate for 5.0% suspension
□0.60 cm diameter tube
△1.27 cm diameter tube
○1.74 cm diameter tube

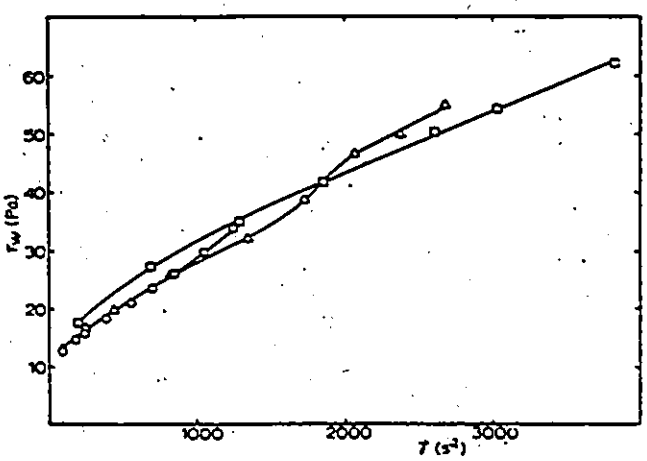

Figure 4.6 Wall shear stress vs. apparent shear rate for 6.0% suspension
□ 0.60 cm diameter tube
△ 1.27 cm diameter tube
○ 1.74 cm diameter tube

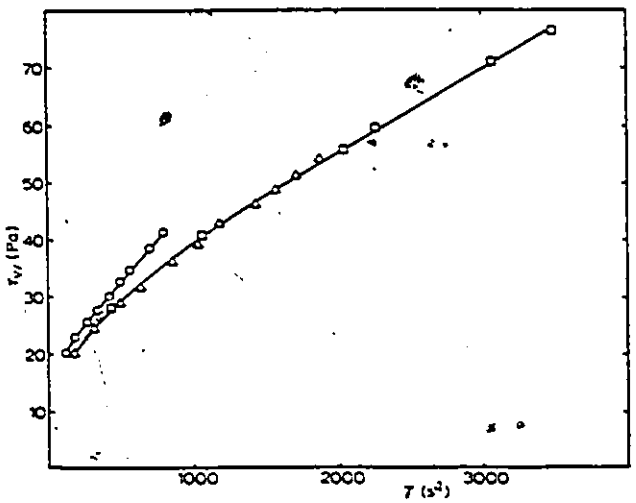

Figure 4.7 Wall shear stress vs. apparent shear rate for 8.0% suspension
□ 0.60 cm diameter tube
△ 1.27 cm diameter tube
○ 1.74 cm diameter tube

CHAPTER 5

DISCUSSION AND CONCLUSIONS

5.1 Newtonian Fluid

The experimental results for the study of 50/50 kerosene in 10W40 agree favourably with theoretical and empirical expectations and establish the fact that the pipe line system can be used successfully to obtain accurate data for Newtonian fluids of low viscosity. The implication of this is that reliable data should be obtained in the same system for non-Newtonian fluids of comparative consistency, as they generally have shorter development lengths.

The shear diagram for the Newtonian oil (Fig. 4.1) is linear over all shear rates for data taken from each of the three test sections, and when extrapolated passed very close to the origin, implying Newtonian behaviour. The variation in fluid viscosity computed from the data for each individual tube was small; the maximum difference for any two tubes being 0.003 Pa·s (Table 4.1). The maximum temperature variation for the tests in all three test sections was 1.1 ^{o}C. This, coupled with variations in measurements of flow rates and pressure drops would be sufficient for causing the three slightly different slopes of the data seen on Fig. 4.1. Fitting the correct straight line through the data would also contribute somewhat to this variation but seems to be quite insignificant. The viscosities determined from the data for each tube

agreed well with Brookfield cone and plate results at essentially the same temperature, again confirming the accuracy of the pipe system.

Friction factors computed using viscosities based on the data from the three tubes agreed well with the anticipated curve for Newtonian fluids in the laminar region. Tests were not extended into the turbulent region as it was originally intended to study all systems in laminar flow only.

5.2 Bentonite Slurries

From the pipe line slurry data it was possible to produce graphs of wall shear stress, τ_w versus the apparent shear rate, $\dot{\gamma}$. It is generally accepted that under quasi-steady conditions, in which the rate of structural change is small, the steady state wall shear stress, $a\Delta P/2L$ is a good approximation. Since the consistency of the curves indicated that the material was in the equilibrium or broken down state, little error would be incurred by plotting these graphs in terms of consistency variables as the material is virtually time independent in this state (i.e., breakdown to equilibrium occurred between successive data readings since sufficient time was allowed after incrementing the pumping rate). These data are plotted on Figures 4.3 through 4.7 for concentrations of 1.96% to 8.0%. The curves are very typical of thixotropic clay materials in the equilibrium state and agree with the description of Smith (1960) and Cheng et al. (1965).

The 1.96% concentration suspension has a very small, if nonexistent yield stress and is virtually a Newtonian fluid in the low shear rate range below 400 s^{-1}, where the data from the three tubes virtually collapsed onto a single curve. Beyond this shear rate transition commences in the 1.27 cm and 1.74 cm diameter tubes as indicated by an increased upward slope of the curves (Fig. 4.3). As expected, transition first occurs in the 1.74 cm diameter tube and is subsequently apparent in the 1.27 cm diameter tube at a higher $\dot{\gamma}$. The 0.60 cm diameter tube data does not indicate distinct transition within the shear rate range shown. A final turbulent region was achieved at higher shear rates in the 1.27 cm diameter tube. Whether or not complete turbulence was reached in the 1.74 cm diameter tube is not obvious from Fig. 4.3, since the output of the pump restricted the flow rate.

Shear diagrams for the 4.0% and 5.0% suspensions (Fig. 4.4 & 4.5) have the same general shape as that for the 1.96% suspension but the value of τ_y is increasing as is the $\dot{\gamma}$ at which turbulence commences. This is expected since as the concentration is increased, the suspension takes on more the characteristics of a Bingham body and the flow becomes plug like.

At concentrations higher than 5% (Fig. 4.6 & 4.7) the degree of thixotropy becomes more pronounced and is evidenced by the spread between the curves at low values of $\dot{\gamma}$. Turbulent flow was not achieved at these concentrations as the solutions

were almost gels and plug flow was very much evident. The transition and turbulent flow regions are not shown on the shear stress graphs for the higher concentrations because the shear rates were not high enough. It is noticeable that the laminar curves change their form from concave to a convex nature as the concentration is increased. This changeover appears to occur at a concentration of about 5%. Furthermore, as the slurry concentration and tube diameter increase, the curves tend to deviate more from the small tube or laminar flow data. This could be due to increased thixotropic behaviour of the system or a scaling effect, indicating that certainly in the smaller diameter range, the diameter has an effect on the shear stress distribution and therefore the flow phenomenon.

Schultz-Grunow (1962) has proposed that at low bentonite concentrations, thixotropy is lost. He found that thixotropic behaviour exists above a concentration of 5% by weight. This is supported by the work of Sharma et al. (1972), who contend that up to C = 5% thixotropic effects are negligible, but not lost. The trends of Figures 4.3 to 4.7 seem to further substantiate these contentions.

For all concentrations, the data from the small (0.60 cm diameter) tube show continuous smooth curves and the flow was apparently in all cases laminar in character. Although a distinct transition region was not observed for the C = 1.96% data for the 0.60 cm diameter tube, it is highly likely, as discussed later, that the flow was in fact turbulent within the shear

rate range under study. Therefore the data from which these curves were produced were used to calculate the apparent viscosity, and subsequently to calculate the flow Reynolds number for the other two tubes. The work of Cheng et al. (1965) certainly indicates that this approach is acceptable, especially for calculating the Reynolds number.

Initially it was hoped to substantiate the shear diagrams with data from a rotating concentric cylinder viscometer which could produce shear rates of up to $2*10^7$ s^{-1}. This apparatus, although not intended for clay slurries, was thought to be quite adequate. Unfortunately, there were small sand inclusions in the clay which caused the cylinders to seize. Increasing the annular gap alleviated this problem but reduced both the range of shear rates and accuracy and also caused end effect difficulties. Brookfield cone and plate and rotating cylinder viscometers did not prove to be adequate, mainly because of low maximum shear rates and jamming due to sand inclusions. Consequently, the data obtained for laminar flows in the 0.60cm diameter tube were used to calculate the apparent viscosities.

The shear stress data for the larger diameter tubes indicate what might be called transition and turbulent regions, with considerable deviations from the smaller tube data. This is more apparent for the C = 1.96% and 4.0% curves (Figures 4.3 and 4.4) when the conditions for turbulence would be exceeded with the pumping rates used. This is also illustrated in

the friction factor vs. Reynolds number curve of Fig. 5.1 which shows that the data agree quite well with the Newtonian fluid curves and indicate that the majority of the data were in fact for the laminar or transitional flow regimes as suspected from the shear diagrams.

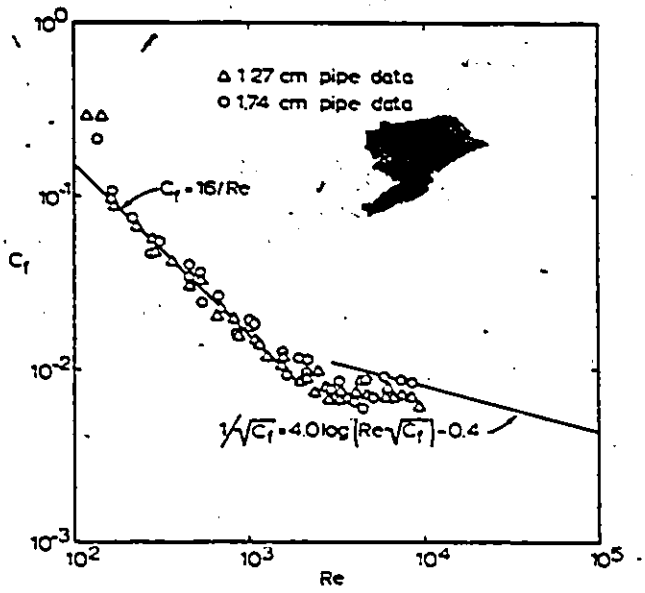

Figure 5.1 Friction factor vs. Reynolds number plot for all concentrations in 1.27 cm and 1.74 cm diameter tubes

Friction factors for the 0.60 cm diameter tube based on the apparent viscosity computed from the 0.60 cm diameter tube data also followed the Newtonian curves. They are not presented on Fig. 5.1 however, as they do not reveal information as to how a relationship between the various tube diameters can be achieved (i.e., the friction factor is computed for a tube size from viscosity data for the same tube size and this

does not indicate how a scaling up technique can be achieved).

The data for the apparent viscosities are shown in Fig. 5.2, the corresponding calculations are summarized in Tables F.1 to F.15 of Appendix F.

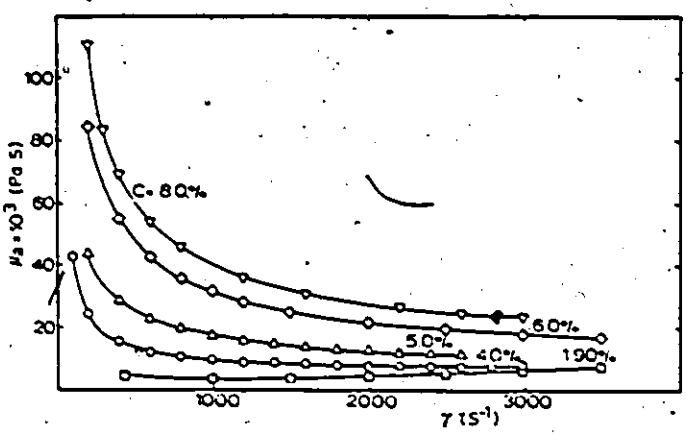

Figure 5.2 Apparent viscosity vs. apparent shear rate for all concentrations at equilibrium in the 0.60 cm diameter tube

The curves are typical of equilibrium state thixotropic materials, all of which show an approach to that of a Bingham plastic for shear rates greater than 2000 s^{-1}. Furthermore, as the bentonite concentration increases, non-Newtonian effects become more pronounced.

Often shear stress data are plotted in the form of a generalized Bingham plastic relationship:

$$\tau - \tau_y = k\dot{\gamma}^n \qquad (5.1)$$

The problem usually is that it is difficult to obtain

τ_y experimentally with any degree of accuracy. However, it was possible to estimate τ_y by extrapolation of the curves to zero $\dot{\gamma}$, a questionable procedure but nonetheless reasonably accurate in the present case, since the data were obtained for relatively low shear rates thus approaching static shear stresses (the feasibility of this procedure is also pointed out by Yalcin and McIntosh, 1961).

On the basis of these τ_y's, a plot of the equilibrium curves for generalized Bingham plastic equations is given in Fig. 5.3, the numerical data are tabulated in Appendix G.

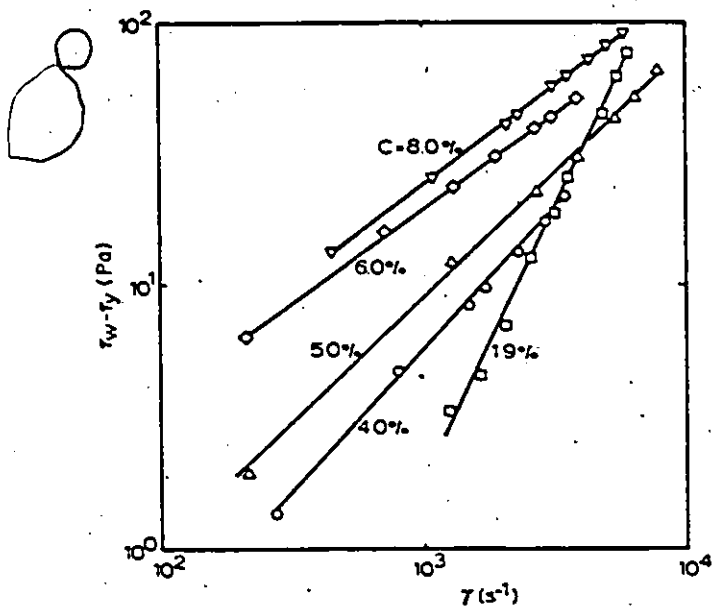

Figure 5.3 Equilibrium curves for bentonite suspensions plotted in the form of the generalized Bingham equation (5.1)

The form of these curves is quite familiar and agrees favourably with the limited available data such as that of Cheng et al. (1965). However the indices 'n' and constants 'k' given in Table 5.1 are quite different to those of Cheng et al.

Table 5.1 Comparison of k and n values for all concentrations

C (%)	τ_y present (Pa)	τ_y (Cheng) (Pa)	n present	- n (Cheng)	- k present ($Pa \cdot s^n$)	k (Cheng) ($Pa \cdot s^n$)
1.7		0.0		0.83		0.0062
1.96	1.0		2.06		1.2 E-06	
4.0	3.5		1.08		3.4 E-03	
4.8		1.6		1.00		0.0086
5.0	7.0		0.93		0.015	
6.0	11.0		0.71		0.145	
7.8		36.0		0.48		2.12
8.0	15.0		0.74		0.148	

This must be attributable to slight differences in the material used since 'n' and 'k' reflect material properties. That is, for $n<1$, the material behaves as a pseudoplastic for which the viscosity decreases with shear rate. However, when $n>1$, the material exhibits dilatant behaviour for which the viscosity increases with shear rate. The differences cannot

be due to thixotropy, since when C=1.96% and thixotropic effects are minimal, there is still no agreement between the data. Furthermore, it cannot be due to the accuracy of τ_y since it is quite small when C=1.96%.

The trend of Cheng's data which go from pseudoplastic through constant apparent viscosity (Bingham plastic) and back to pseudoplastic as concentration increases is perhaps more difficult to comprehend than the data presented here.

Graphs of hydraulic power consumption per unit length of pipe vs. Reynolds number based on apparent viscosity taken from the 0.60 cm diameter tube are shown on Figures 5.4 and 5.5.

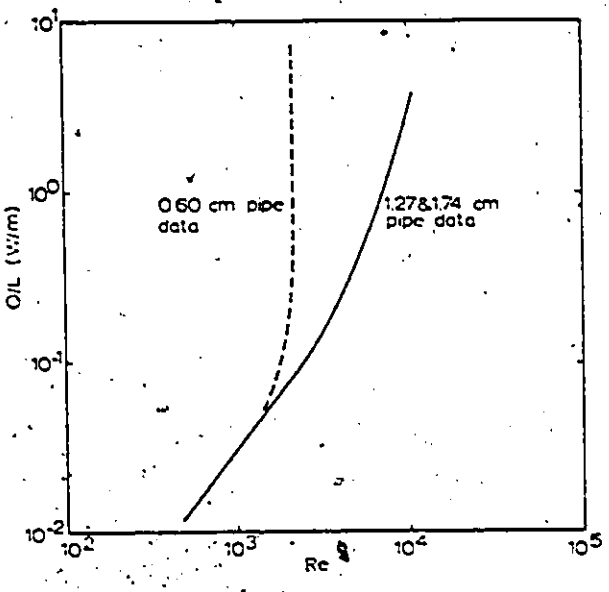

Figure 5.4 Power requirement per unit length of tube vs. Reynolds number for 1.96% concentration

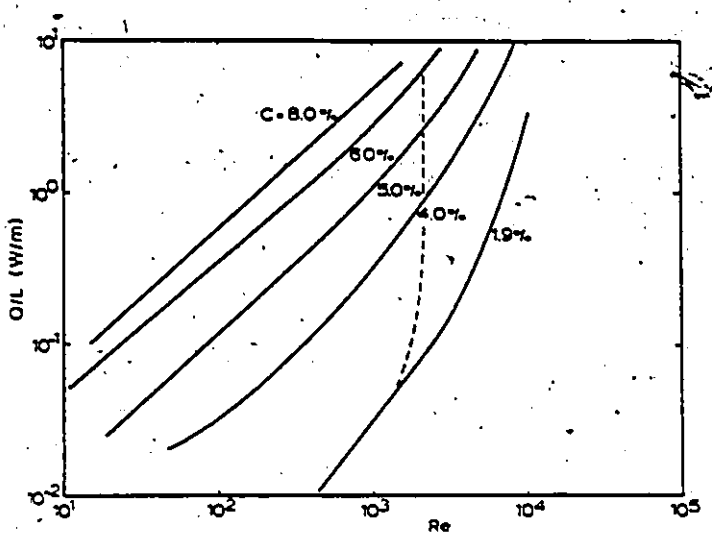

Figure 5.5 Smoothed power requirement curves in all 3 tubes for all concentrations vs. Reynolds number

It was generally apparent that the power consumption was not greatly affected by the diameter of the tube for a given Reynolds number as the curves for all three tubes at a given concentration tended to collapse onto one line. As the concentration was reduced it was apparent that diameter does have a marked effect as evidenced by the smoothed curves of Fig. 5.4 for C = 1.96% which shows that the D = 0.60 cm curve diverges and assymptotically approaches a condition for which the power increases with virtually no effect on Reynolds number. As this is for the small tube data, it may relate to the condition for calculating the apparent viscosity. The small tube data for C = 1.96% shows a concave curve assymptotically approaching a constant Reynolds number of about 2000 (the onset of transition). This may indicate that the flow of the 1.96%

suspension is much like that of dirty water in the turbulent region.

It may be postulated that perhaps all of the curves approach a limiting Reynolds number Re^*, depending on the fluid concentration and tube diameter. Unfortunately the data are not extensive enough to indicate what effect the concentration and diameter have on the limiting Re^*, at least for C greater than 1.96%. These curves do not indicate power requirements as a function of flow rate, which can easily be calculated. However the limiting Re^* may be a useful criteria i.e., Re is constant for Q/L greater than Q/L_{Re^*}.

The smoothed specific power consumption curves for all the data are summarized on Fig. 5.5.

5.3 Conclusions and Recommendations for Future Studies

The rheology of time dependent fluids has to this point been considered an experimental science and as such the area is open to question and criticism. Explicit rheological models have not been developed to cover the vast spectrum of time dependent fluids because of the many material parameters involved and difference in experimental techniques employed. Any further data or insight which can be added to the literature constitutes a contribution even if it only raises more unanswered questions.

The purpose of this work was to make evident the fact that the rheology of non-Newtonian fluids has yet to be fully

understood and that the many correlation techniques offered in the literature to date, which involve tedious calculations, may not be much more accurate at predicting internal flow behaviour than the method suggested herein.

There have been several correlation techniques presented to date for describing non-Newtonian pipe flow (Dodge and Metzner, 1959, Cheng et al., 1965, Kemblowski and Kolodziejski, 1973, and Heywood and Richardson, 1978) all of which are cumbersome to use for general design purposes. Some techniques may be more accurate and fit the data better than others for a given criteria, but when applied to the vast number of different slurries imaginable, it is not anticipated that one method is more representative. This work presents an easy to use method of obtaining results and the data substantiate the general aspects of the limited available data for the pumping of slurries, in particular that of Cheng et al. (1965). The C_f vs. Re diagram of Fig. 5.1 is in good agreement with that of Cheng et al. for similar bentonite slurries and also reflects the results of Kemblowski and Kolodziejski for aqueous suspensions of kaolin and those of Heywood and Richardson for similar materials.

It would seem that for the majority of practical cases, the slurry would be fully stressed and in an equilibrium state, with the exception of transient flow through valves and fittings etc. and therefore would behave as if it were a generalized Bingham plastic as described by Equation 5.1. The measure-

ments indicate that for internal flows, clay slurries with concentrations between 1.96% and 8.0% may be treated as Bingham plastics for the majority of practical purposes, and that thixotropic effects are minimal for normal shear rates. This is especially true for bentonite suspensions of less than 5% concentration by weight. Also for laminar, transition and low Reynolds number turbulent flows, the friction factor curves for Newtonian fluid flows in smooth pipes can be used with reasonable accuracy for all concentrations and pipe diameters, provided the laminar apparent viscosity is used when calculating the Reynolds number.

Furthermore, the specific pumping energy loss varies as a function of Reynolds number and is generally diameter independent at higher concentrations. There seems to be a scaling effect for small diameter tubes, but this should be very minimal or nonexistent for larger diameter pipes. Lastly, there appears to be uncertainty in the values of the constants for the generalized Bingham equation and their relationship to concentration, which may be due to the fact that they are much affected by the nature of the material and makeup of the slurry.

Pipe line data for thixotropic systems are limited and much further work needs to be done before substantial rheological models can be produced. A starting point might possibly be the observation of change of material structure along a pipe which is pressure tapped at close intervals along its

length. The difference in pressure drop between the successive measuring points gives a clear indication of how the material is behaving in the pipe (buildup or breakdown of structure with time). It would also give a clear indication as to what point in the flow the material reaches its equilibrium structure and what effect the relaxation time has in transient flows.

Experimental data of many investigators has indicated that, whereas the region of transitional flow of Newtonian fluids occurs within a narrow Reynolds number range, the flow of non-Newtonian systems in the transitional range occurs over a very wide range of Reynolds numbers. Due to the opposing views with regard to the range of transitional flow of these fluids and to the method of calculating the coefficients of flow resistance in transitional and turbulent flow, an extension of this work aimed directly at studying these regions would be of great value.

Further viscometric studies should also be continued for the above reasons and also to confirm the nature of the equilibrium shear diagrams of Figures 4.3 to 4.7. This would not only help to substantiate the pipe line data (as in the case of Cheng et al.), but a general correlation of a simple form between viscometer data and pipe line data for a given fluid at any concentration would aid in simplifying pipe line design.

Finally another interesting aspect to be considered

would be the pulsatile pumping of such slurries. The work of Round et al. (1976), on the pulsatile pumping of sand type slurries indicated that at low pulsing frequencies of the order of 1 - 2 Hertz, the power consumption requirements compared with that of continuous pumping are reduced. It is therefore suggested that, especially for the higher concentrations when the slurry becomes a gel, that pulsatile flow be considered for more economical pumping of such slurries.

REFERENCES

1. Alves, G. E., D. F. Boucher and R. L. Pigford, "Pipe-Line Design for Non-Newtonian Solutions and Suspensions", Chem. Eng. Progress, 48, pp. 385, (1952).

2. Bauer, W. H., and E. A. Collins, "Rheology", F. R. Eirich, ed., Vol. 4, Chapt. 8, pp. 423, Academic Press, New York, (1967).

3. Bingham, E. C. and H. Green, "Paint, A Plastic Material and not a Viscous Liquid; The Measurement of its Mobility and Yield Value", Proc. Am. Soc. Test. Mat., 19, pp. 640, (1919).

4. Bogue, D. C., "Entrance Effects and Prediction of Turbulence in Non-Newtonian Flow", Ind. Eng. Chem., 51, pp. 874, (1959).

5. Buckingham, E., "On Plastic Flow Through Capillary Tubes", Proc. Am. Soc. Test. Mat., 21, pp. 1154, (1921).

6. Caldwell, D. H. and H. E. Babbitt, "Flow of Muds, Sludges, and Suspensions in Circular Pipe", Ind. Eng. Chem., 33, pp. 249, (1941).

7. Cheng, D. C.-H., D. J. Ray and F. H. H. Valentin, "The Flow of Thixotropic Bentonite Suspensions Through Pipes and Pipe Fittings", Trans. Instn. Chem. Engrs., 43, pp. T176, (1965).

8. Dean, J. A., ed., "Lange's Handbook of Chemistry", Eleventh Ed., McGraw-Hill, Inc., (1973).

9. Dodge, D. W. and A. B. Metzner, "Turbulent Flow of Non-Newtonian Systems", A. I. Ch. E. Journal, 5, pp. 189, (1959).

10. Fredrickson, A. G., "A Model for the Thixotropy of Suspensions", A. I. Ch. E. Journal, 16, pp. 436, (1970).

11. Freundlich, H. and H. L. Roder, "Dilatancy and its Relation to Thixotropy", Trans. Far. Soc., 34, pp. 383, (1939).

12. Gaybrysh, A. F., T. Ree, H. Eyring, N. McKee and I. Cutler, "Flow Properties of Attapulgite Suspensions in Water", Trans. Soc. Rheology, 5, pp. 67, (1961).

13. Goodeve, C. F. and G. W. Whitfield, "The Measurement of Thixotropy in Absolute Units", Trans. Far. Soc., 34, pp. 511, (1908).

14. Goodeve, C. F., "A General Theory of Thixotropy and Viscosity", Trans. Far. Soc., 35, pp. 342, (1939).

15. Green, H. and R. N. Weltmann, "Analysis of the Thixotropy of Pigment-Vehicle Suspensions", Ind. Eng. Chem. Anal. Ed., 15, pp. 201, (1943).

16. Green, H. and R. N. Weltmann, "The Effect of Thixotropy on Plasticity Measurements", J. App. Physics, 15, pp. 414, (1944).

17. Green, H. and R. N. Weltmann, "Equations of Thixotropic Breakdown for the Rotational Viscometer", Ind. Eng. Chem., 18, pp. 67, (1946).

18. Hahn, S. J., T. Ree and H. Eyring, "Flow Mechanism of Thixotropic Substances", Ind. Eng. Chem., 51, pp. 856, (1959).

19. Hedstrom, B. O. A., "Flow of Plastics Materials in Pipes", Ind. Eng. Chem., 44, pp. 651, (1952).

20. Heywood, N. I. and J. F. Richardson, "Rheological Behavior of Flocculated and Dispersed Aqueous Kaolin Suspensions in Pipe Flow", J. Rheology, 22, pp. 599, (1978).

21. Hoffman, R. L., "Discontinuous and Dilatant Viscosity Behavior in Concentrated Suspensions", Trans. Soc. Rheology, 16, pp. 155, (1972).

22. Joye, D. D. and G. W. Poehlein, "Characteristics of Thixotropic Behavior", Trans. Soc. Rheology, 15, pp. 51, (1971).

23. Kemblowski, Z. and J. Kolodziejski, "Flow Resistances of Non-Newtonian Fluids in Transitional and Turbulent Flow", Inter. Chem. Eng., 13, pp. 265, (1973).

24. Leonard, J. T. and R. N. Hazlett, "Rheology of Thixotropic Suspensions of Magnesium Montmorillonite", Ind. Eng. Chem. Fundamentals, 5, pp. 233, (1966).

25. McMillen, E. L., "Simplified Pressure-Loss Calculations for Plastic Flow", Chem. Eng. Progress, 44, pp. 537, (1948).

26. Metzner, A. B., "Pipe-Line Design for Non-Newtonian Fluids", Chem. Eng. Progress, 50, pp. 27, (1954).

27. Metzner, A. B. and J. C. Reed, "Flow of Non-Newtonian Fluids - Correlation of the Laminar, Transition and Turbulent - flow Regions", A. I. Ch. E. Journal, 1, pp. 434, (1955).

28. Metzner, A. B. and M. Whitlock, "Flow Behavior of Concentrated (Dilatant) Suspensions", Trans. Soc. Rheology, 2, pp. 239, (1958).

29. Mooney, M., "Explicit Formulas for Slip and Fluidity", J. Rheology, 2, pp. 210, (1931).

30. Oldroyd, J. G., "The Interpretation of Observed Pressure Gradients in Laminar Flow of Non-Newtonian Liquids Through Tubes", J. Colloid Sci., 4, pp. 333, (1949).

31. Perry, R. H. and C. H. Chilton, "Chemical Engineer's Handbook", Fifth Ed., McGraw-Hill, Inc., (1973).

32. Reiner, M., "The Theory of Plastic Flow in the Rotational Viscometer", J. Rheology, 1, pp. 6, (1929).

33. Reiner, M., "Deformation and Flow", H. K. Lewis & Co., London, (1949).

34. Reynolds, O., "Dilatancy", Nature, 33, pp. 429, (1896).

35. Round, G. F., B. Latto and K. Y. Lau, "Pulsating Flows of Solid-Liquid Suspensions", Proceedings of Hydrotransport 4, pub. by BHRA., (May, 1976).

36. Schultz-Grunow, F., "Contribution to Thixotropy", Progress in International Research on Thermodynamic and Transport Properties Second Symposium on Thermophysical Properties, A. S. M. E., Academic Press, New York, pp. 718, (1962).

37. Sharma, P. V., R. Nagarajan and G. S. Davies, "Flow Behaviour of Time-Dependent Bentonite-Water Suspensions", Powder Technol., 6, pp. 103, (1972).

38. Sharma, P. V., R. Nagarajan and G. S. Davies, "Flow Behaviour of Bentonite-Water Suspensions in a Horizontal Pipe", Powder Technol., 8, pp. 193, (1973).

39. Smith, R. W., "Flow of Limestone and Clay Slurries in Pipelines", A. I. M. E. Trans., 217, pp. 258, (1960).

40. Street, N., "Viscosity of Clay Suspensions", World Oil, 147, pp. 151, (1958).

41. Thomas, D. G., "Significant Aspects of Non-Newtonian Technology", Progress in International Research on Thermodynamic and Transport Properties Second Symposium on Thermophysical Properties, A. S. M. E., Academic Press, New York, pp. 669, (1962).

42. Verwey, E. J. W. and J. H. deBoer, "Dilatancy", Rec. Trav. Chim., 57, pp. 383, (1939).

43. Weltmann, R. N., "Breakdown of Thixotropic Structure as a Function of Time", J. App. Physics, 14, pp. 343, (1943).

44. Weltmann, R. N., "Friction Factors for Flow of Non-Newtonian Materials in Pipelines", Ind. Eng. Chem., 48, pp. 386, (1956).

45. Wilhelm, R. H., D. M. Wroughton and W. F. Loeffel, "Flow of Suspensions Through Pipes", Ind. Eng. Chem., 31, pp. 622, (1939).

46. Wilkinson, W. L., "Non-Newtonian Fluids", Pergamon Press, (1960).

47. Williamson, R. V., "The Flow of Pseudoplastic Materials", Ind. Eng. Chem., 21, pp. 1108, (1929).

48. Winding, C. C., G. P. Baumann and W. L. Kranich, "Flow Properties of Pseudoplastic Fluids - Part I", Chem. Eng. Progress, 43, pp. 527, (1947)[1].

49. Winding, C. C., G. P. Baumann and W. L. Kranich, "Flow Properties of Pseudoplastic Fluids - Part II", Chem. Eng. Progress, 43, pp. 613, (1947)[2].

50. Yalcin, A. S. and R. McIntosh, "Some Rheological Parameters of Clays and Their Thixotropic Behavior", The Canadian Journal of Chem. Eng., 39, pp. 76, (1961).

APPENDIX A

VISCOSITY AND ITS CONNOTATIONS

The term viscosity as used in the literature seems to have various connotations dependent upon the particular author using the term and the particular fluid system under study.

Viscosity as it is applied to Newtonian fluids has only one meaning. It is the constant of proportionality relating shear rate to shear stress in equation (1.1):

$$\tau = -\mu du/dr = \mu\dot{\gamma}$$

It is called the coefficient of viscosity or simply viscosity and is the slope of the shear diagram. Since this is linear for a Newtonian fluid, the viscosity is constant at a given temperature and pressure.

When dealing with non-Newtonian systems however, the term viscosity may have one of several meanings since it may not have a constant value in the rheological equation relating τ and $\dot{\gamma}$. The meaning of viscosity must now be quantified. Consider the shear diagrams of Fig. A.1. Curve A represents a Newtonian fluid of constant viscosity. Curve B represents typical pseudoplastic flow which approaches Newtonian behaviour at high rates of shear. How should the viscosity of this fluid be defined? As in the case of Newtonian fluids, the ratio of $\tau/\dot{\gamma}$ has the units of viscosity

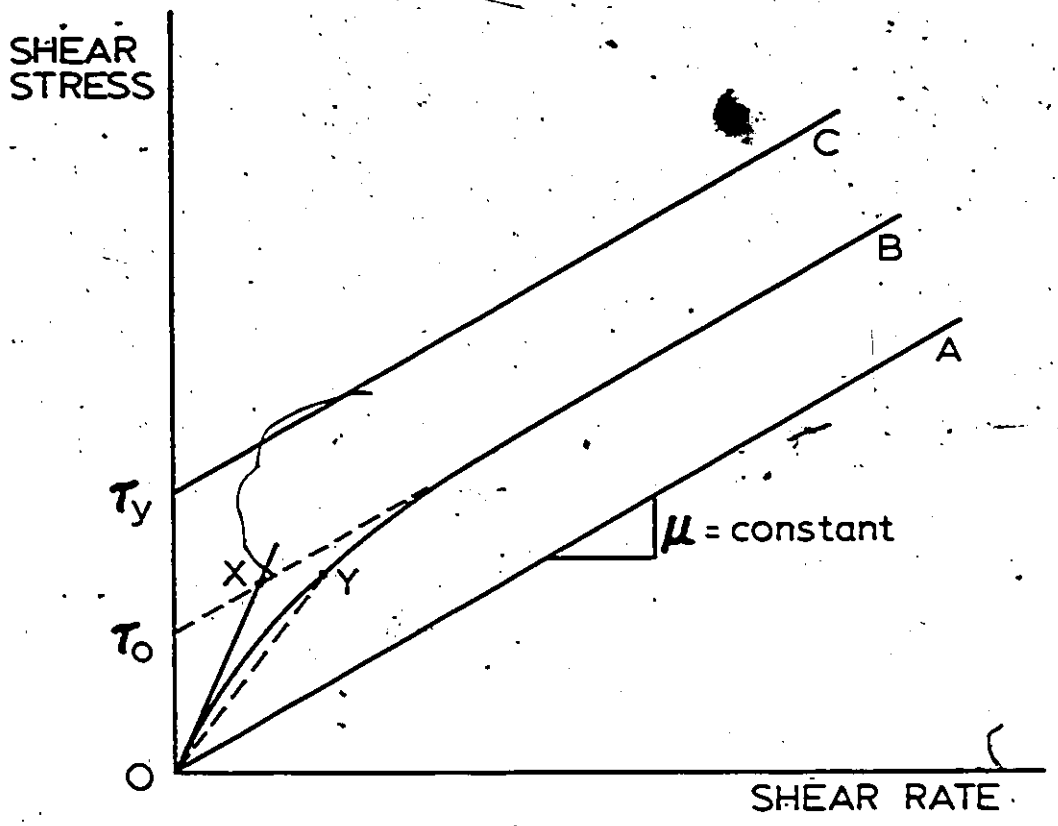

Figure A.1 Typical non-Newtonian shear diagram.

and at any point Y along the curve this is called the apparent viscosity, μ_a at the rate of shear involved:

$$\mu_a = \frac{\text{shear stress at Y}}{\text{shear rate at Y}} = \text{slope of OY}$$

Hence the apparent viscosity of a pseudoplastic decreases with shear rate and is not a constant value. In a similar fashion apparent viscosity increases with shear rate for a dilatant material.

The value of the apparent viscosity defined in this manner must lie between two well defined limits. Experimental work has indicated that the curve passes through the origin

so that the first infinitesimal increment of stress must produce a rate of shear such that the resulting apparent viscosity is equal to the slope of the tangent OX to the curve at zero rate of shear or:

$$\lim_{\dot{\gamma}\to 0} \mu_a = \mu_0$$

defining the viscosity at zero shear, μ_0.

In a like manner, the other limit of the apparent viscosity (as $\dot{\gamma}\to\infty$) must be defined by the slope of the straight line $\tau_0 B$. This limit is designated as the viscosity at infinite rate of shearing or limiting viscosity, μ_∞ (this has an equivalent value for a dilatant fluid except that τ_0 would be replaced by a $\dot{\gamma}_0$). Generally, the two limits of viscosity are dependent upon the system and its temperature but not on the rate of shear or flow and not on the dimensions of the flow tube. This makes these viscosities particularly useful in correlating data for pseudoplastic fluids. The apparent viscosity is dependent upon the system temperature and rate of shear, and its value varies between the two limits of viscosity. For a given pseudoplastic or dilatant fluid, temperature and pipe, the apparent viscosity is a function of flow velocity. This complicates the use of the apparent viscosity since a complete shear diagram must be known for every sample considered.

The other definition of viscosity (plastic viscosity, μ_p) has been considered in the treatment of Bingham plastics

(μ_p is the slope of the line $\tau_y C$). Note that an apparent viscosity at any shear rate can also be defined for a Bingham plastic (Street, 1958).

APPENDIX B

DESIGN OF THE TEST SECTIONS

B.1 Determination of Test Section Lengths From Pressure Drop Data

The pressure drop per unit length in the three test sections (nominally 0.25 in, 0.5 in and 0.625 in diameter) can be determined from the Hagen-Poiseuille equation for laminar Newtonian flows in circular pipes. The pressure drops were first calculated for the maximum Reynolds number in laminar flow (about 2000), and were based on viscosities of roughly 1, 10, 30, 50, 80 and 100 centipoise for appropriate aqueous solutions of glycerol. The relevant properties of glycerol in aqueous solution can be found in the handbooks of Perry and Chilton (1973) and Dean (1973). All calculations are based on a working temperature of 25°C.

Table B.1 Properties of aqueous glycerol at 25°C*

% Glycerol by Weight	Abs. Viscosity (g/cm·s)	Abs. Viscosity ($lb_m/ft \cdot s$)	Density (g/cm^3)	Density (lb_m/ft^3)
10.00	1.153E-02	0.775E-03	1.02070	63.722
62.00	10.11 E-02	6.794E-03	1.15655	72.203
76.00	30.56 E-02	20.536E-03	1.19465	74.582
81.00	51.02 E-02	34.285E-03	1.20810	75.422
85.00	81.5 E-02	54.768E-03	1.21870	76.083
87.00	106.1 E-02	71.299E-03	1.22400	76.414

*taken from Perry and Chilton (1973) and Dean (1973)

Table B.2 Kinematic viscosities of glycerol solutions

%Glycerol by Weight	Kinematic Viscosity (μ/ρ)	
	(cm^2/s)	(ft^2/s)
10.00	1.13E-02	0.012E-03
62.00	8.74E-02	0.094E-03
76.00	25.58E-02	0.275E-03
81.00	42.23E-02	0.455E-03
85.00	66.87E-02	0.720E-03
87.00	86.68E-02	0.933E-03

Table B.3 Nominal test section dimensions

Tube dia. (ft)	Tube radius (ft)	Tube area (ft^2)
0.02083	0.0104	3.39E-04
0.04167	0.0208	1.36E-03
0.05208	0.0260	2.12E-03
Tube dia. (cm)	**Tube radius (cm)**	**Tube area (cm^2)**
0.635	0.3175	0.317
1.270	0.6350	1.267
1.587	0.7937	1.979

Table B.4 Velocity and flow rates for various glycerol solutions in the test sections

% Glycerol by Weight	Nominal Tube Dia. (in)	Velocity u_m (ft/s)	$q = u_m * a$ (ft^3/s)	u_m (cm/s)	q (cm^3/s)
10%	0.250	1.152	3.917E-04	35.57	11.265
	0.500	0.576	0.783E-03	17.79	22.54
	0.625	0.461	0.977E-03	14.05	27.67
62%	0.250	9.025	30.685E-04	275.27	87.178
	0.500	4.512	6.136E-03	137.53	174.377
	0.625	3.610	7.653E-03	110.03	216.733
76%	0.250	26.433	89.608E-04	805.68	253.77
	0.500	13.213	17.970E-03	402.73	508.91
	0.625	10.572	22.413E-03	322.23	634.74
81%	0.250	43.649	147.970E-04	1330.42	419.05
	0.500	21.819	29.674E-03	665.04	840.37
	0.625	17.458	37.011E-03	532.12	1048.15
85%	0.250	69.112	234.290E-04	2106.53	663.51
	0.500	34.548	46.980E-03	1053.02	1330.47
	0.625	27.642	58.600E-03	842.53	1659.55
87%	0.250	89.582	303.680E-04	2730.46	864.62
	0.500	44.780	60.900E-03	1364.89	1729.50
	0.625	35.829	75.960E-03	1092.07	2151.19

The pressure drop per unit length of pipe (L) can be calculated from the Hagen-Poiseuille equation for Newtonian laminar flow:

$$\Delta P/L = 8\mu q/\pi a^4 g_c$$

Table B.5 Pressure drops per unit length of tube

Viscosity (centipoise)	% Glycerol by Weight	Nominal Tube Dia. (in)	$\Delta P/L$ (lb_f/ft^3)	$\Delta P/L$ (g/cm^3)	$\Delta P/L$ (lb_f/in^3)
1.153	10%	0.250	2.052	0.0332	1.19E-03
		0.500	0.256	4.15E-03	1.48E-04
		0.625	0.131	2.10E-03	7.58E-05
10.11	62%	0.250	140.930	2.2540	0.0815
		0.500	17.613	0.2817	0.0102
		0.625	8.997	0.1441	0.0052
30.56	76%	0.250	1243.980	19.9280	0.7200
		0.500	155.920	2.4978	0.0902
		0.625	79.646	1.2760	0.0461
51.02	81%	0.250	3429.480	54.9400	1.9850
		0.500	429.840	6.8860	0.2488
		0.625	219.570	3.5175	0.1271
81.50	85%	0.250	8674.240	138.9610	5.0207
		0.500	1087.220	17.4170	0.6293
		0.625	555.350	8.8967	0.3214
106.10	87%	0.250	14681.500	234.5700	8.4750
		0.500	1834.600	29.3250	1.0595
		0.625	937.160	15.0133	0.5424

Table B.6 Summary of results for Re = 2000, θ = 25°C

% Glycerol by Weight	Viscosity (centipoise)	Nominal Tube Dia. (in)	Velocity (ft/s)	q (U.S. $\frac{gal}{min}$)	ΔP/L ($\frac{lb_f}{in^3}$)
10%	1.153	0.250	1.152	0.176	1.19E-03
		0.500	0.576	0.351	1.48E-04
		0.625	0.461	0.438	7.58E-05
62%	10.11	0.250	9.025	1.377	0.0815
		0.500	4.512	2.754	0.0102
		0.625	3.610	3.435	0.0052
76%	30.56	0.250	26.433	4.022	0.7200
		0.500	13.213	8.065	0.0902
		0.625	10.572	10.060	0.0461
81%	51.02	0.250	43.649	6.641	1.9850
		0.500	21.819	13.319	0.2488
		0.625	17.458	16.612	0.1271
85%	81.50	0.250	69.112	10.516	5.0207
		0.500	34.548	21.088	0.6293
		0.625	27.642	26.301	0.3214
87%	106.10	0.250	89.582	13.671	8.4750
		0.500	44.780	27.334	1.0595
		0.625	35.829	34.093	0.5424

Table B.7 Summary of results for Re = 1000, θ = 25°C

% Glycerol by Weight	Viscosity (centipoise)	Nominal Tube Dia. (in)	Velocity (ft/s)	q $\left(\text{U.S. } \frac{\text{gal}}{\text{min}}\right)$	$\Delta P/L$ $\left(\frac{\text{lb}_f}{\text{in}^3}\right)$
10%	1.153	0.250	0.576	0.088	5.95E-04
		0.500	0.288	0.176	7.40E-05
		0.625	0.230	0.219	3.80E-05
62%	10.11	0.250	4.512	0.686	0.0407
		0.500	2.256	1.377	0.0051
		0.625	1.805	1.717	0.0026
76%	30.56	0.250	13.216	2.011	0.3600
		0.500	6.608	4.033	0.0451
		0.625	5.286	5.030	0.0230
81%	51.02	0.250	21.824	3.321	0.9925
		0.500	10.909	6.659	0.1245
		0.625	8.729	8.306	0.0635
85%	81.50	0.250	34.556	5.258	2.5170
		0.500	17.278	10.546	0.3145
		0.625	13.821	13.151	0.1607
87%	106.10	0.250	44.791	6.815	4.2480
		0.500	22.390	13.667	0.5310
		0.625	17.915	17.046	0.2711

i) Determination of Entrance Lengths

For Newtonian fluids, the entrance length, L_e is approximately given by:

$$L_e/D = 0.029Re$$

assuming that the fluid enters the pipe with a flat velocity profile (Wilkinson, 1960). For each nominal tube diameter an estimated entrance length is calculated and tabulated below for Re = 2000.

Table B.8 Estimated upper limits on entrance lengths

Nominal Tube Diameter (in)	L_e (in)	L_e (cm)
0.250	14.50	36.83
0.500	29.00	73.66
0.625	36.25	92.07

These lengths represent upper bounds on the value of L_e and serve only as guide lines since the flow will be developed to some extent by the time it reaches the test sections (the velocity profile will not be flat as the equation assumes). In general turbulent flows and non-Newtonian flows have shorter development lengths as the velocity profiles are blunter (Bogue, 1959). The actual entrance lengths of the pipe system were all roughly as long as or longer than those listed in Table B.8.

ii) Determination of Test Section Lengths

The distance between pressure taps on each test

section is determined primarily by two factors:

1) The maximum length of glass tubing that the test section can be obtained in (there are standard lengths for these diameters).

2) The magnitude (or range in magnitude) of the anticipated pressure drops to be measured between the pressure taps. This is primarily dependent on the range of pressures that a particular pressure sensing device can detect (in this case a differential manometer).

Test section lengths chosen for each diameter of tubing are given below.

A) 0.60 cm I.D. Tubing (0.25 in nominal)

The maximum length of the tubing available is four feet and the diameter is listed as 0.60 cm $\pm$ 0.02 cm. Each end can be fitted with a quick fit connector by the glass blower.

Table B.9 Anticipated pressure drops in 0.60 cm dia. tube at Re = 2000

Section Length (inches)	Pressure Drop (lb_f/in^2)	
	Minimum Fluid Viscosity (10.11 centipoise)	Maximum Fluid Viscosity (106.10 centipoise)
48	3.9	407.8
30	2.4	254.9
20	1.6	169.9
15	1.2	127.4

Above 30 inches the maximum pressure drop gets quite high and below 30 inches the minimum values get quite small (especially for smaller Reynolds numbers) hence, 30 inches (76.2 cm) was the chosen pressure tap separation in the 0.60 cm diameter tube.

B) 1.27 cm I.D. Tubing (0.50 in nominal)

The maximum available length of the tubing is again four feet and the diameter is listed as 1.25 cm $\pm$ 0.02 cm. Again each end can be adapted to fit into the flow system.

Table B.10 Anticipated pressure drops in 1.27 cm dia. tube at Re = 2000

Section Length (inches)	Pressure Drop (lb_f/in^2)	
	Minimum Fluid Viscosity (10.11 centipoise)	Maximum Fluid Viscosity (106.10 centipoise)
48	0.49	51.0
40	0.41	42.4
30	0.31	31.8
20	0.20	21.2
15	0.15	15.9

Since the distance between pressure taps cannot be the maximum of 48 inches and some clearance must be left between the taps and the quick fit ends, 40 inches (101.6 cm) was the chosen test section length.

C) 1.74 cm I.D. Tubing (0.625 in nominal)

This section was purchased as a standard 5 foot glass pipe length and had only to be pressure tapped.

Table B.11 Anticipated pressure drops in 1.74 cm dia. tube at Re = 2000

Section Length (inches)	Pressure Drop (lb_f/in^2)	
	Minimum Fluid Viscosity (10.11 centipoise)	Maximum Fluid Viscosiy (106.10 centipoise)
50	0.26	27.1
40	0.21	21.7
30	0.16	16.3
20	0.10	10.8
15	0.08	8.1

The 50 inch (127.0 cm) section length was chosen to give the largest possible minimum pressure drop and still avoid placing the taps too close to the ends of the pipe.

APPENDIX C

DETERMINATION OF TEST SECTION DIAMETERS

The mean diameter of each test section was determined prior to having them pressure tapped by filling the tubes with a known volume (weight) of mercury and then measuring the height of the Hg column. The first set of data for each tube was obtained by filling the tube at one end and the second set by filling from the other end. A mean diameter was then calculated.

Table C.1 Mean diameter calculation of 0.60 cm dia. tube

	Data 1	Data 2
Volume of Mercury (cm^3)	8.0	19.0
Height of Mercury (cm)	28.10	66.60
Weight of Hg (g)	108.18	256.93
Temperature Hg (^oC)	29.7	29.6
Density Hg (g/cm^3)	13.5224	13.5227
$D = (4v/\pi L)^{0.5}$ (cm)	0.602	0.603
Mean Diameter (cm)	0.60	

Table C.2 Mean diameter calculation of 1.27 cm dia. tube

	Data 1	Data 2
Volume of Mercury (cm^3)	40.0	80.0
Height of Mercury (cm)	31.20	62.60
Weight of Hg (g)	540.90	1081.74
Temperature Hg (^oC)	29.7	29.9
Density Hg (g/cm^3)	13.5224	13.5219
$D = (4v/\pi L)^{0.5}$ (cm)	1.275	1.274
Mean Diameter (cm)	1.27	

Table C.3 Mean diameter calculation of 1.74 cm dia. tube

	Data 1	Data 2
Volume of Mercury (cm^3)	50.0	80.0
Height of Mercury (cm)	21.70	32.30
Weight of Hg (g)	676.15	1081.75
Temperature Hg (^oC)	29.5	29.9
Density Hg (g/cm^3)	13.5229	13.5219
$D = (4v/\pi L)^{0.5}$ (cm)	1.713	1.776
Mean Diameter (cm)	1.74	

Table C.4 Density of mercury at various temperatures*

Temperature (^{o}C)	Density (g/cm^{3})
28	13.5266
29	13.5242
30	13.5217
31	13.5193

* Values of density used in Tables C.1 to C.3 are interpolated from this chart at appropriate temperatures.

APPENDIX D

NEWTONIAN PIPE-LINE TEST DATA

The results of the experiments carried out in each of the three test sections for the Newtonian oil 50/50 kerosene in 10W40 are summarized.

D.1 Newtonian Oil Data Sheets

Data Sheets-50/50 kerosene in 10W40

Table D.1 Test results for 0.60 cm dia. tube

Test Number	Efflux Time (seconds)	Volume (cm^3)	q_{avg} (cm^3/s)	ΔP_{avg} (in Hg)	$Temp_{avg}$ (^oC)
133	26.70	770	28.84	4.10	21.2
134	18.60	876	47.10	6.45	21.0
135	12.75	918	72.00	9.80	21.2
136	8.90	859	96.52	12.52	21.4
137	7.65	903	118.04	15.77	21.5
138	6.25	917	146.72	19.25	21.8
139	5.20	881	169.42	22.70	22.0
140	4.95	950	191.92	26.05	22.4

Table D.2 Test results for 1.27 cm dia. tube

Test Number	Efflux Time (seconds)	Volume (cm^3)	q_{avg} (cm^3/s)	ΔP_{avg} (in Hg)	$Temp_{avg}$ ($^{\circ}C$)
85	7.30	938	129.65	1.31	19.2
	6.65	870			
87	6.10	941	154.00	1.52	19.3
	5.85	899			
89	4.85	917	188.35	1.87	19.7
	4.60	863			
92	4.20	950	226.05	2.22	20.2
	4.20	949			
94	3.50	890	254.20	2.46	20.5
	3.90	991			
96	3.30	940	283.85	2.81	20.9
	3.10	877			
99	3.10	1000	643.30	3.12	21.5
	2.90	930			
101	2.50	887	356.80	3.43	21.9
	2.55	915			
104	2.40	978	403.35	3.87	22.2
	2.40	958			
106	2.10	937	446.00	4.18	22.7
	1.90	847			

Table D.3 Test results for 1.74 cm dia. tube

Test Number	Efflux Time (seconds)	Volume (cm^3)	q_{avg} (cm^3/s)	ΔP_{avg} (in Hg)	$Temp_{avg}$ (^oC)
141	4.40	860	195.30	0.68	21.9
	4.45	869			
143	3.50	835	237.45	0.84	21.9
	3.50	827			
145	3.55	909	516.90	0.93	22.0
	3.40	887			
147	2.80	860	307.30	1.10	21.9
	3.05	938			
149	2.50	930	368.30	1.31	21.9
	2.40	875			
151	2.30	897	394.00	1.53	21.9
	2.10	836			
153	2.00	950	477.50	1.79	22.3
	2.00	960			
155	1.80	928	523.00	1.98	21.4
	1.80	955			

D.2 Newtonian Oil Data Analysis

Data Analysis-50/50 kerosene in 10W40

Table D.4 Shear stress calculations for 0.60 cm dia. tube

Test Number	$\Delta P_{corrected}$ (cm Hg)	$\Delta P/L_{corrected}$ (kPa/m)	$\frac{4q}{a^3\pi}$ (s^{-1})	$\frac{a\Delta P}{2L}$ (Pa)
133	9.78	17.12	1344.5	25.76
134	15.39	26.94	2199.0	40.55
135	23.39	40.93	3361.4	61.57
136	30.55	53.46	4505.3	80.44
137	37.64	65.86	5509.1	99.11
138	45.95	80.40	6849.0	120.99
139	54.18	94.80	7909.8	142.68
140	62.17	108.79	8959.3	163.70

Table D.5 Shear stress calculations for 1.27 cm dia. tube

Test Number	$\Delta P_{corrected}$ (cm Hg)	$\Delta P/L_{corrected}$ (kPa/m)	$\frac{4q}{a^3\pi}$ (s^{-1})	$\frac{a\Delta P}{2L}$ (Pa)
85	3.13	4.10	634.6	13.07
87	3.63	4.76	751.6	15.18
89	4.46	5.86	922.0	18.67
92	5.30	6.95	1106.6	22.17
94	5.87	7.71	1244.7	24.61
96	6.71	8.80	1394.5	28.12
99	7.45	9.77	1574.7	31.17
101	8.19	10.74	1747.0	34.28
104	9.24	12.12	1974.7	38.69
106	10.00	13.12	2183.8	41.89

Table D.6 Shear stress calculations for 1.74 cm dia. tube

Test Number	$\Delta P_{corrected}$ (cm Hg)	$\Delta P/L_{corrected}$ (kPa/m)	$\frac{4q}{a^3 \pi}$ (s^{-1})	$\frac{a\Delta P}{2L}$ (Pa)
141	1.62	1.70	375.4	7.42
143	2.00	2.10	456.3	9.14
145	2.22	2.33	496.7	10.15
147	2.62	2.75	590.6	12.02
149	3.13	3.28	707.8	14.32
151	3.65	3.80	757.2	16.57
153	4.27	4.48	917.7	19.53
155	4.73	4.96	1004.9	21.64

Table D.7 Friction factor-Reynolds number calculations for 0.60 cm dia. tube

Test Number	u_m (m/s)	C_f	Re
133	1.012	0.060	284.0
134	1.655	0.035	464.5
135	2.529	0.023	710.0
136	3.390	0.017	951.6
137	4.146	0.014	1163.7
138	5.153	0.011	1446.7
139	5.951	0.010	1670.6
140	6.741	0.009	1892.4

Table D.8 Friction factor-Reynolds number calculations for 1.27 cm dia. tube

Test Number	u_m (m/s)	C_f	Re
85	1.012	0.030	542.3
87	1.199	0.025	642.3
89	1.471	0.020	787.9
92	1.766	0.017	945.6
94	1.986	0.015	1063.6
96	2.225	0.013	1191.7
99	2.512	0.012	1345.6
101	2.788	0.010	1492.9
104	3.151	0.009	1687.5
106	3.484	0.008	1866.2

Table D.9 Friction factor-Reynolds number calculations for 1.74 cm dia. tube

Test Number	u_m (m/s)	C_f	Re
141	0.818	0.026	570.1
143	0.994	0.022	693.0
145	1.082	0.021	754.3
147	1.287	0.017	896.9
149	1.542	0.014	1074.9
151	1.650	0.014	1149.9
153	2.000	0.012	1393.6
155	2.190	0.011	1526.1

APPENDIX E

BENTONITE SLURRY PIPELINE TEST DATA

The results of the experiments carried out in each of the three test sections for the five bentonite slurry concentrations are summarized.

E.1 Bentonite Slurry Compositions - Table E.1

Concentration of Bentonite by Weight	Weight of Water (grams)	Weight of Bentonite (gm)	ρ_{avg} $\left(\frac{g}{cm^3}\right)$	T_{avg} (^{o}C)
1.96%	21000.0	419.8	1.000	23.0
4.0%	20000.0	833.3	1.005	20.0
5.0%	18000.0	947.4	1.012	21.8
6.0%	19000.0	1212.8	1.010	25.0
8.0%	17000.0	1478.3	1.018	24.2

E.2 Bentonite Slurry Data Sheets

Data Sheets-1.96% bentonite by weight

Table E.2 Test results for 0.60 cm dia. tube

Test Number	Efflux Time (seconds)	Volume (cm^3)	q_{avg} (cm^3/s)	ΔP_{avg} (in Hg)	$Temp_{avg}$ (^{o}C)
305	31.60	298	9.36	0.30	24.8
	36.60	340			
307	24.10	630	26.08	0.70	24.6
	24.20	630			
309	20.30	717	34.90	0.90	24.5
	20.65	712			

Table E.2 continued...

Test Number	Efflux Time (seconds)	Volume (cm^3)	q_{avg} (cm^3/s)	ΔP_{avg} (in Hg)	$Temp_{avg}$ (^oC)
311	18.15 15.65	804 686	44.06	1.30	24.0
313	14.15 14.50	766 775	53.79	2.22	24.0
315	11.65 11.65	783 772	66.74	3.18	23.8
317	10.95 10.95	820 827	75.20	4.32	23.7
319	10.05 9.95	875 868	87.15	5.83	23.4
321	7.85 8.65	790 888	101.65	7.40	23.4
323	6.60 7.60	760 885	115.80	10.20	23.4
325	6.25 6.40	793 823	127.73	12.25	23.5

Table E.3 Test results for 1.27 cm dia. tube

Test Number	Efflux Time (seconds)	Volume (cm^3)	q_{avg} (cm^3/s)	ΔP_{avg} (in Hg)	$Temp_{avg}$ (^oC)
327	12.15	710	58.69	0.15	22.7
	13.35	787			
329	8.25	760	92.39	0.25	22.5
	8.45	783			
331	6.75	840	125.03	0.40	22.4
	6.75	848			
333	5.00	808	160.34	0.74	22.3
	5.50	875			
335	4.20	836	197.87	1.00	22.4
	4.50	885			
337	3.90	900	230.92	1.25	22.5
	3.70	855			
339	3.40	877	258.97	1.53	22.5
	3.50	910			
341	2.80	840	299.61	1.84	22.4
	2.60	778			
343	2.40	803	333.94	2.25	22.5
	2.40	800			
345	2.10	785	374.11	2.66	22.6
	2.15	805			
893	6.10	2830	463.98	3.99	25.2
	6.95	3225			
895	5.50	2788	504.89	4.68	25.6
	5.20	2615			
898	5.30	2858	539.12	5.17	25.6
	5.00	2695			
900	4.40	2620	594.37	6.10	25.6
	4.32	2563			

Table E.4 Test results for 1.74 cm dia. tube

Test Number	Efflux Time (seconds)	Volume (cm^3)	q_{avg} (cm^3/s)	ΔP_{avg} (in CCl_4)	$Temp_{avg}$ (^oC)
347	12.05 11.00	767 700	63.64	2.45	24.6
349	8.45 7.95	790 750	93.91	3.15	24.0
351	5.95 5.80	835 828	141.55	4.28	24.2
353	4.60 4.80	812 838	175.55	5.20	24.5
354	3.70 3.60	860 833	232.41	7.10	24.6
356	3.00 3.30	795 869	264.16	10.57	24.7
358	2.65 2.80	770 815	290.82	13.90	24.9
360	2.70 2.60	865 836	320.95	16.46	25.1
363	2.30 2.50	850 930	370.78	20.15	25.5
364	2.20 2.30	905 935	408.94	24.50	25.5
				ΔP_{avg} (in Hg)	
913	6.45 5.68	3216 2817	497.27	1.50	25.5
916	5.20 6.00	2975 3450	573.55	1.81	25.5
919	4.87 5.00	3205 3288	657.85	2.20	25.5

Data Sheets-4.0% bentonite by weight

Table E.5 Test results for 0.60 cm dia. tube

Test Number	Efflux Time (seconds)	Volume (cm^3)	q_{avg} (cm^3/s)	ΔP_{avg} (in Hg)	$Temp_{avg}$ (^oC)
705	40.25	266	6.78	0.75	23.2
	47.50	330			
708	36.05	705	19.54	1.27	23.0
	33.80	660			
711	19.60	720	36.69	1.83	22.5
	21.50	788			
713	18.20	775	42.60	2.04	22.4
	15.95	680			
715	12.50	711	56.04	2.60	22.3
	14.00	773			
717	10.25	734	71.82	3.21	22.0
	10.55	760			
719	8.70	740	85.53	3.92	22.0
	8.00	688			
721	8.15	785	95.41	5.65	22.0
	8.00	756			
723	7.20	751	103.27	6.57	22.0
	7.10	726			
725	6.45	756	116.72	9.50	22.0
	6.65	773			
727	6.20	805	130.10	12.12	22.0
	5.50	717			

Table E.6 Test results for 1.27 cm dia. tube

Test. Number	Efflux Time (seconds)	Volume (cm^3)	q_{avg} (cm^3/s)	ΔP_{avg} (in Hg)	$Temp_{avg}$ (^oC)
940	12.35 12.85	750 785	60.91	0.60	23.4
942	7.30 7.50	800 837	110.59	0.80	23.2
944	4.70 5.30	790 888	167.81	1.01	23.0
946	3.90 3.90	887 890	227.81	1.30	23.0
948	7.20 7.30	2170 2237	303.91	2.22	23.0
950	6.20 7.00	2295 2650	374.36	3.25	22.8
952	5.30 6.50	2245 2768	424.71	4.10	23.0
954	5.00 5.20	2423 2530	485.57	5.07	23.0
957	5.30 5.10	2740 2640	517.31	5.61	23.5
959	5.10 4.38	2838 2435	556.20	6.68	23.5

Table E.7 Test results for 1.74 cm dia. tube.

Test Number	Efflux Time (seconds)	Volume (cm^3)	q_{avg} (cm^3/s)	ΔP_{avg} (in Hg)	$Temp_{avg}$ (^oC)
962	11.00	740	68.18	0.43	21.2
	10.45	722			
964	7.50	777	102.83	0.49	21.0
	7.75	791			
966	5.75	820	142.53	0.54	20.8
	6.10	869			
970	4.10	882	215.97	0.72	20.8
	4.10	889			
972	3.40	1005	296.73	0.85	20.8
	3.30	983			
974	5.90	2240	379.04	1.05	20.8
	6.58	2490			
977	5.70	2645	461.60	1.19	20.8
	4.90	2250			
980	4.80	2498	521.98	1.39	20.4
	4.80	2513			
982	4.50	2575	573.08	1.81	20.5
	4.30	2468			
986	3.60	2315	642.77	2.49	20.5
	4.00	2570			
989	3.60	2492	692.03	3.06	20.5
	3.80	2629			
992	3.60	2690	745.04	3.40	20.0
	3.85	2860			

Data Sheets-5.0% bentonite by weight

Table E.8 Test results for 0.60 cm dia. tube

Test Number	Efflux Time (seconds)	Volume (cm^3)	q_{avg} (cm^3/s)	ΔP_{avg} (in Hg)	$Temp_{avg}$ (^oC)
994	46.00	202	4.54	1.44	26.2
	55.70	261			
996	22.80	610	27.10	3.18	26.2
	25.50	700			
998	15.15	857	57.18	4.77	25.7
	13.65	789			
1001	9.65	790	82.09	6.10	25.7
	11.15	918			
1003	7.50	851	114.63	8.06	25.5
	7.60	880			
1005	6.20	842	136.19	9.46	25.4
	6.15	841			
1008	5.20	850	163.20	11.55	25.2
	5.10	831			
1010	5.20	950	183.50	16.72	25.6
	5.10	940			

Table E.9 Test results for 1.27 cm dia. tube

Test Number	Efflux Time (seconds)	Volume (cm^3)	q_{avg} (cm^3/s)	ΔP_{avg} (in Hg)	$Temp_{avg}$ (^oC)
1013	22.95	510	22.39	0.83	23.6
	21.50	485			
1015	13.30	730	55.52	0.99	23.4
	12.75	716			
1017	10.35	890	86.10	1.22	23.2
	10.45	901			
1019	7.60	910	119.87	1.42	23.0
	8.00	960			
1022	4.40	850	192.65	1.75	23.2
	4.70	903			
1025	3.75	1020	271.00	2.14	23.0
	3.40	918			
1027	5.20	1835	352.45	2.68	23.0
	5.17	1820			
1030	4.10	1908	462.78	4.96	23.0
	5.30	2439			
1032	4.20	2240	534.95	6.62	23.0
	4.10	2200			
1034	3.40	2104	618.02	8.01	23.0
	3.60	2222			

Table E.10 Test results for 1.74 cm dia. tube

Test Number	Efflux Time (seconds)	Volume (cm^3)	q_{avg} (cm^3/s)	ΔP_{avg} (in Hg)	$Temp_{avg}$ (^oC)
1037	11.45	849	73.66	0.87	21.8
	10.25	750			
1039	7.10	972	138.81	1.08	21.8
	6.95	978			
1041	4.30	896	208.35	1.30	21.9
	4.32	900			
1045	3.30	1000	304.54	1.49	22.0
	3.30	1010			
1048	6.30	2228	357.41	1.65	22.0
	5.95	2149			
1051	5.00	2125	435.41	1.89	22.1
	4.80	2140			
1053	4.90	2575	525.60	2.15	22.1
	4.20	2208			
1056	4.20	2400	574.49	2.35	22.0
	4.10	2368			
1058	3.80	2428	637.66	2.56	22.0
	3.63	2310			
1061	3.20	2273	710.87	2.79	22.0
	3.50	2490			
1064	3.40	2500	735.50	3.12	21.8
	3.50	2575			
1067	3.30	2650	804.69	3.25	21.8
	3.15	2540			
1069	3.00	2564	852.33	3.40	21.8
	3.40	2890			

Data Sheets-6.0% bentonite by weight

Table E.11 Test results for 0.60 cm dia. tube

Test Number	Efflux Time (seconds)	Volume (cm^3)	q_{avg} (cm^3/s)	ΔP_{avg} (in Hg)	$Temp_{avg}$ (^oC)
1125	48.70	210	4.44	2.81	25.8
	42.00	192			
1128	33.40	489	15.04	4.37	25.8
	40.05	618			
1130	21.80	620	27.83	5.64	25.8
	27.00	735			
1132	20.30	810	40.02	6.71	25.7
	19.45	781			
1134	15.25	860	56.42	8.11	25.7
	15.55	878			
1136	13.15	860	65.46	8.76	25.7
	13.40	878			
1138	10.35	857	82.35	9.99	25.7
	10.45	856			

Table E.12 Test results for 1.27 cm dia. tube

Test Number	Efflux Time (seconds)	Volume (cm^3)	q_{avg} (cm^3/s)	ΔP_{avg} (in Hg)	$Temp_{avg}$ (^oC)
1100	25.40	498	19.65	1.33	25.5
	26.60	524			
1102	14.95	780	52.58	1.68	25.5
	14.85	787			
1104	9.50	868	91.16	2.00	25.0
	9.85	896			
1106	5.90	1008	170.33	2.62	25.2
	5.40	917			
1109	3.15	869	276.44	3.24	25.2
	3.35	928			
1111	5.40	1925	354.05	3.92	25.2
	6.45	2268			
1113	5.95	2520	424.26	4.72	25.5
	5.60	2380			
1115	5.00	2450	487.84	5.07	25.5
	4.05	1967			
1117	4.10	2250	550.00	5.56	25.5
	4.66	2563			

Table E.13 Test results for 1.74 cm dia. tube

Test Number	Efflux Time (seconds)	Volume (cm^3)	q_{avg} (cm^3/s)	ΔP_{avg} (in Hg)	$Temp_{avg}$ (^oC)
1072	17.25	850	49.48	1.16	25.5
	16.90	840			
1074	10.10	932	93.78	1.33	26.3
	9.55	910			
1076	7.45	970	131.03	1.45	26.3
	7.00	923			
1078	4.60	929	203.28	1.69	26.2
	4.55	931			
1080	3.20	940	293.76	1.95	26.1
	3.37	990			
1083	7.50	2765	368.07	2.18	25.8
	6.15	2260			
1085	5.30	2355	444.38	2.39	25.8
	6.10	2711			
1088	5.00	2730	547.89	2.75	25.5
	4.90	2694			
1091	4.45	2908	652.05	3.12	25.5
	4.07	2648			

Data Sheets-8.0% bentonite by weight

Table E.14 Test results for 0.60 cm dia. tube

Test Number	Efflux Time (seconds)	Volume (cm^3)	q_{avg} (cm^3/s)	ΔP_{avg} (in Hg)	$Temp_{avg}$ (^oC)
510	56.10	527	9.48	4.58	26.8
	57.20	548			
512	33.10	758	23.06	6.58	26.1
	32.50	755			
514	17.00	750	44.06	8.97	26.2
	17.95	790			
516	16.35	791	48.82	9.62	25.7
	17.25	850			
518	14.35	945	66.12	11.48	26.1
	12.50	830			
520	12.00	904	75.49	12.42	25.8
	11.95	904			
522	10.00	923	91.64	13.90	26.0
	9.35	850			
524	9.15	968	105.54	15.36	25.8
	9.45	995			
526	7.60	944	122.41	16.91	25.6
	8.00	965			
528	6.70	938	138.70	18.57	26.0
	6.55	900			

Table E.15 Test results for 1.27 cm dia. tube

Test Number	Efflux Time (seconds)	Volume (cm^3)	q_{avg} (cm^3/s)	ΔP_{avg} (in Hg)	$Temp_{avg}$ (^oC)
530	19.80 19.05	730 725	37.46	2.07	26.5
532	13.55 13.15	890 875	66.11	2.51	26.0
534	8.75 8.45	910 872	103.59	2.95	25.8
536	7.15 7.30	960 960	132.88	3.24	25.9
538	5.70 5.10	1013 900	177.09	3.68	25.8
540	4.70 4.50	1010 945	212.44	4.00	25.9
542	4.20 3.70	1020 905	243.72	4.35	26.1
545	3.40 3.25	1005 950	293.95	4.70	26.4
548	3.10 2.85	998 920	322.37	4.94	26.2
550	2.70 2.60	948 910	350.55	5.20	26.0
553	2.50 2.40	955 930	384.75	5.50	26.0

Table E.16 Test results for 1.74 cm dia. tube

Test Number	Efflux Time (seconds)	Volume (cm^3)	q_{avg} (cm^3/s)	ΔP_{avg} (in Hg)	$Temp_{avg}$ (^oC)
555	12.45	848	68.92	1.90	22.5
	11.80	823			
557	8.50	855	100.46	2.14	21.7
	8.85	888			
559	6.65	941	141.27	2.40	21.8
	6.70	945			
561	5.20	930	179.01	2.60	22.0
	4.80	860			
564	3.70	830	223.64	2.82	22.0
	3.70	825			
567	3.20	838	260.77	3.06	22.0
	3.10	805			
569	3.00	880	294.77	3.24	22.0
	3.10	910			
571	2.20	810	363.64	3.46	22.0
	2.25	808			
574	2.25	835	370.00	3.59	22.0
	2.25	830			
577	2.10	900	418.79	3.85	22.0
	2.20	900			

E.3 Bentonite Slurry Data Analysis

Data Analysis-1.96% bentonite by weight

Table E.17 Shear stress calculations for 0.60 cm dia. tube

Test Number	$\Delta P_{corrected}$ (cm Hg)	$\Delta P/L_{corrected}$ (kPa/m)	$\frac{4q}{a^3}$ (s^{-1})	$\frac{a\Delta P}{2L}$ (Pa)
305	0.71	1.24	437.0	1.87
307	1.65	2.89	1217.6	4.36
309	2.11	3.69	1629.4	5.55
311	3.07	5.38	2057.2	8.09
313	5.23	9.15	2511.3	13.79
315	7.49	13.11	3115.9	19.73
317	10.16	17.78	3511.1	26.76
319	13.74	24.04	4068.8	36.20
321	17.42	30.49	4745.7	45.87
323	24.00	42.00	5406.4	63.20
325	28.83	50.44	5963.6	75.89

Table E.18 Shear stress calculations for 1.27 cm dia. tube

Test Number	$\Delta P_{corrected}$ (cm Hg)	$\Delta P/L_{corrected}$ (kPa/m)	$\frac{4q}{a^3\pi}$ (s^{-1})	$\frac{a\Delta P}{2L}$ (Pa)
327	0.35	0.46	288.3	1.47
329	0.59	0.77	453.9	2.47
331	0.94	1.24	612.2	3.94
333	1.74	2.28	787.7	7.28
335	2.35	3.09	972.0	9.85
337	2.94	3.86	1134.4	12.30
339	3.60	4.73	1272.2	15.07
341	4.33	5.68	1471.8	18.12
343	5.30	6.95	1640.5	22.15
345	6.26	8.21	1837.8	26.18
893	9.40	12.34	2279.3	39.32
895	11.03	14.47	2480.3	46.12
898	12.17	15.97	2648.5	50.90
900	14.35	18.83	2920.1	60.02

Table E.19 Shear stress calculations for 1.74 cm dia. tube

Test Number	$\Delta P_{corrected}$ (cm CCl_4)	$\Delta P/L_{corrected}$ (kPa/m)	$\frac{4q}{a^3\pi}$ (s^{-1})	$\frac{a\Delta P}{2L}$ (Pa)
347	2.32	0.28	122.6	1.24
349	2.99	0.36	180.8	1.60
351	4.05	0.50	272.6	2.17
353	4.91	0.60	338.1	2.63
354	6.73	0.83	447.6	3.60
356	10.00	1.23	508.7	5.35
358	13.14	1.61	560.1	7.03
360	15.57	1.91	618.1	8.34
363	19.08	2.35	714.0	10.22
364	23.19	2.85	787.5	12.42
	$\Delta P_{corrected}$ (cm Hg)			
913	3.53	3.71	957.9	16.14
916	4.28	4.50	1115.3	19.58
919	5.18	5.44	1266.3	23.77

Data Analysis-4.0% bentonite by weight

Table E.20 Shear stress calculations for 0.60 cm dia. tube

Test Number	$\Delta P_{corrected}$ (cm Hg)	$\Delta P/L_{corrected}$ (kPa/m)	$\frac{4q}{a^3\pi}$ (s^{-1})	$\frac{a\Delta P}{2L}$ (Pa)
705	1.76	3.09	264.2	4.88
708	2.99	5.23	781.8	8.28
711	4.31	7.54	1468.0	11.92
713	4.82	8.44	1701.8	13.36
715	6.12	10.71	2273.3	16.95
717	7.53	13.17	2862.1	20.88
719	9.18	16.06	3399.6	25.42
721	13.18	23.06	3849.7	36.53
723	15.41	26.97	4168.6	42.76
725	22.83	39.94	4684.6	63.30
727	28.48	49.83	5189.4	78.95

Table E.21 Shear stress calculations for 1.27 cm dia. tube.

Test Number	$\Delta P_{corrected}$ (cm Hg)	$\Delta P/L_{corrected}$ (kPa/m)	$\frac{4q}{a^3\pi}$ (s^{-1})	$\frac{a\Delta P}{2L}$ (Pa)
940	1.41	1.85	299.2	5.91
942	1.88	2.47	543.2	7.87
944	2.38	3.12	824.4	9.94
946	3.06	4.02	1119.2	12.64
948	5.22	6.86	1493.0	21.86
950	7.65	10.04	1839.1	31.99
952	9.65	12.66	2086.4	40.35
954	11.93	15.66	2385.4	49.92
957	13.20	17.33	2541.3	55.23
959	15.72	20.63	2733.6	65.76

Table E.22 Shear stress calculations for 1.74 cm dia. tube

Test Number	$\Delta P_{corrected}$ (cm Hg)	$\Delta P/L_{corrected}$ (kPa/m)	$\frac{4q}{a^3\pi}$ (s^{-1})	$\frac{a\Delta P}{2L}$ (Pa)
962	1.01	1.06	131.3	4.62
964	1.15	1.21	198.0	5.27
966	1.27	1.33	274.2	5.81
970	1.69	1.78	415.9	7.75
972	2.00	2.10	571.4	9.14
974	2.47	2.59	730.1	11.30
977	2.80	2.94	889.0	12.81
980	3.27	3.43	1005.2	14.96
982	4.26	4.47	1103.6	19.48
986	5.86	6.15	1237.9	26.79
988	7.20	7.56	1332.7	32.93
992	8.00	8.40	1434.8	36.58

Data Analysis - 5.0% bentonite by weight

Table E.23 Shear stress calculations for 0.60 cm dia. tube

Test Number	$\Delta P_{corrected}$ (cm Hg)	$\Delta P/L_{corrected}$ (kPa/m)	$\frac{4q}{a^3\pi}$ (s^{-1})	$\frac{a\Delta P}{2L}$ (Pa)
994	3.39	5.93	212.0	8.92
996	7.48	13.09	1265.2	19.70
998	11.23	19.64	2669.8	29.56
1001	14.36	25.12	3832.8	37.80
1003	18.97	33.19	5351.7	49.94
1005	22.26	38.96	6358.5	58.62
1008	27.18	47.56	7619.3	71.57
1010	39.35	68.86	8567.1	103.63

Table E.24 Shear stress calculations for 1.27 cm dia. tube

Test Number	$\Delta P_{corrected}$ (cm Hg)	$\Delta P/L_{corrected}$ (kPa/m)	$\frac{4q}{a^3\pi}$ (s^{-1})	$\frac{a\Delta P}{2L}$ (Pa)
1013	1.95	2.56	110.0	8.17
1015	2.33	3.06	272.8	9.74
1017	2.87	3.77	423.0	12.01
1019	3.34	4.39	588.9	13.98
1022	4.12	5.40	946.4	17.22
1025	5.04	6.61	1331.3	21.07
1027	6.31	8.28	1731.9	26.38
1030	11.67	15.32	2273.4	48.83
1032	15.58	20.44	2628.0	65.16
1034	18.85	24.74	3036.1	78.86

Table E.25 Shear stress calculations for 1.74 cm dia. tube

Test Number	$\Delta P_{corrected}$ (cm Hg)	$\Delta P/L_{corrected}$ (kPa/m)	$\frac{4\bar{q}}{a^3\pi}$ (s^{-1})	$\frac{a\Delta P}{2L}$ (Pa)
1037	2.05	2.15	141.8	9.38
1039	2.54	2.67	267.3	11.63
1041	3.06	3.21	401.2	13.98
1045	3.51	3.68	586.5	16.04
1048	3.88	4.08	681.1	17.76
1051	4.45	4.67	838.9	20.35
1053	5.06	5.31	1012.2	23.13
1056	5.53	5.80	1106.4	25.28
1058	6.02	6.32	1228.5	27.53
1061	6.56	6.89	1369.0	30.02
1064	7.34	7.71	1416.4	33.56
1067	7.65	8.03	1549.7	34.95
1069	8.12	8.53	1641.4	37.15

Data Analysis-6.0% bentonite by weight

Table E.26 Shear stress calculations for 0.60 cm dia. tube

Test Number	$\Delta P_{corrected}$ (cm Hg)	$\Delta P/L_{corrected}$ (kPa/m)	$\frac{4q}{a^3\pi}$ (s^{-1})	$\frac{a\Delta P}{2L}$ (Pa)
1125	6.61	11.57	207.3	17.41
1128	10.28	18.00	701.9	27.08
1130	13.27	23.22	1299.3	34.95
1132	15.79	27.63	1868.6	41.58
1134	19.08	33.40	2634.3	50.25
1136	20.61	36.07	3056.1	54.28
1138	23.51	41.14	3844.9	61.91

Table E.27 Shear stress calculations for 1.27 cm dia. tube

Test Number	$\Delta P_{corrected}$ (cm Hg)	$\Delta P/L_{corrected}$ (kPa/m)	$\frac{4q}{a^3\pi}$ (s^{-1})	$\frac{a\Delta P}{2L}$ (Pa)
1100	3.13	4.11	96.6	13.09
1102	3.95	5.19	258.3	16.54
1104	4.71	6.18	447.8	19.69
1106	6.17	8.09	836.8	25.80
1109	7.62	10.01	1358.0	31.90
1111	9.22	12.11	1739.3	38.59
1113	11.11	14.58	2084.2	46.46
1115	11.93	15.66	2396.5	49.91
1117	13.09	17.17	2701.9	54.74

Table E.28 Shear stress calculations for 1.74 cm dia. tube

Test Number	$\Delta P_{corrected}$ (cm Hg)	$\Delta P/L_{corrected}$ (kPa/m)	$\frac{4q}{a^3\pi}$ (s^{-1})	$\frac{a\Delta P}{2L}$ (Pa)
1072	2.73	2.87	95.3	12.49
1074	3.13	3.28	180.6	14.32
1076	3.41	3.58	252.3	15.60
1078	3.98	4.18	391.5	18.19
1080	4.59	4.82	565.8	20.99
1083	5.13	5.39	708.8	23.46
1085	5.62	5.90	856.1	25.72
1088	6.47	6.79	1055.1	29.59
1091	7.34	7.71	1255.9	33.58

Data Analysis-8.0% bentonite by weight

Table E.29 Shear stress calculations for 0.60 cm dia. tube

Test Number	$\Delta P_{corrected}$ (cm Hg)	$\Delta P/L_{corrected}$ (kPa/m)	$\frac{4q}{a^3\pi}$ (s^{-1})	$\frac{a\Delta P}{2L}$ (Pa)
510	10.78	18.86	442.6	28.38
512	15.49	27.10	1076.6	40.78
514	21.11	36.94	2057.0	55.59
516	22.64	39.61	2279.2	59.61
518	27.01	47.27	3086.9	71.14
520	29.23	51.14	3524.4	76.96
522	32.71	57.24	4278.4	86.14
524	36.15	63.25	4927.3	95.18
526	39.79	69.63	5714.9	104.79
528	43.70	76.47	6475.5	115.07

Table E.30 Shear stress calculations for 1.27 cm dia. tube

Test Number	$\Delta P_{corrected}$ (cm Hg)	$\Delta P/L_{corrected}$ (kPa/m)	$\frac{4q}{a^3\pi}$ (s^{-1})	$\frac{a\Delta P}{2L}$ (Pa)
530	4.87	6.39	184.0	20.38
532	5.91	7.75	324.8	24.72
534	6.94	9.11	508.9	29.04
536	7.62	10.01	652.8	31.90
538	8.66	11.36	869.9	36.22
540	9.41	12.35	1043.6	39.38
542	10.24	13.44	1197.3	42.83
545	11.06	14.51	1444.0	46.26
548	11.62	15.26	1583.7	48.63
550	12.24	16.06	1722.1	51.19
553	12.94	16.99	1890.1	54.15

Table E.31 Shear stress calculations for 1.74 cm dia. tube

Test Number	$\Delta P_{corrected}$ (cm Hg)	$\Delta P/L_{corrected}$ (kPa/m)	$\frac{4q}{a^3\pi}$ (s^{-1})	$\frac{a\Delta P}{2L}$ (Pa)
555	4.47	4.70	132.7	20.45
557	5.04	5.29	193.5	23.03
559	5.65	5.93	272.0	25.83
561	6.12	6.42	344.7	27.98
564	6.64	6.97	430.7	30.35
567	7.20	7.56	502.2	32.93
569	7.62	8.00	567.7	34.87
571	8.14	8.55	700.3	37.24
574	8.45	8.87	712.5	38.63
577	9.06	9.51	806.5	41.43

APPENDIX F

BENTONITE SLURRY DATA CORRELATIONS

Calculations of apparent viscosity, friction factor, power consumption and Reynolds number are summarized. The wall shear stress was obtained from the shear diagram at a given shear rate in the 0.60 cm diameter for each case. A sufficient number of appropriate points were then chosen to cover the shear rate ranges in the 1.27 cm and 1.74 cm tubes. The friction factor in each tube was based upon the apparent viscosity obtained in the 0.60 cm tube, other parameters such as length and diameter pertain to the particular tube under study. This is also true for the Reynolds number. The power consumption per unit length of tube was calculated as described in Chapter 3.

Data Correlations-1.96% bentonite by weight

Table F.1 Data correlations for 0.60 cm dia. tube

$\dot{\gamma}$ (s^{-1})	τ_w (Pa)	μ_a (Pa·s) $*10^3$	C_f	$Re*10^{-3}$	Q/L (W/m)
437	1.87	4.27	0.0346	0.463	1.161
500	2.06	4.12	0.0291	0.550	1.465
1000	3.35	3.35	0.0184	1.351	4.769
1500	5.51	3.67	0.0086	1.850	11.754
2000	8.47	4.24	0.0075	2.137	24.121
2500	13.02	5.21	0.0074	2.173	46.334
3000	19.06	6.35	0.0075	2.139	81.357
3500	26.09	7.45	0.0073	2.125	129.970
4000	33.75	8.44	0.0074	2.146	192.151
4500	42.85	9.52	0.0075	2.139	274.428
5000	52.95	10.59	0.0075	2.137	376.805
5500	65.35	11.88	0.0076	2.096	511.545
5964	75.89	12.72	0.0075	2.122	644.045

Table F.2 Data correlations for 1.27 cm dia. tube

$\dot{\gamma}$ (s^{-1})	τ_w (Pa)	μ_a (Pa·s) $*10^3$	C_f	$Re*10^{-3}$	Q/L (W/m)
288	1.47	5.11	0.0140	1.145	2.713
500	2.06	4.12	0.0098	2.466	9.937
750	2.63	3.51	0.0087	4.340	29.807
1000	3.35	3.35	0.0079	6.061	63.894
1250	4.31	3.45	0.0072	7.367	114.639
1500	5.51	3.67	0.0069	8.299	182.969
1750	6.80	3.88	0.0062	9.152	270.167
1837	7.37	4.01	0.0061	9.305	307.216

Table F.3 Data correlations for 1.74 cm dia. tube

$\dot{\gamma}$ (s^{-1})	τ_w (Pa)	μ_a (Pa·s) $*10^3$	C_f	$Re*10^{-3}$	Q/L (W/m)
123	1.24	10.12	0.0348	0.459	1.810
200	1.38	6.94	0.0184	1.092	4.163
300	1.58	5.27	0.0116	2.160	8.816
400	1.84	4.61	0.0087	3.291	15.751
500	2.06	4.12	0.0089	4.605	31.391
600	2.35	3.91	0.0091	5.820	55.474
700	2.51	3.59	0.0087	7.392	84.694
787	2.78	3.52	0.0085	8.471	116.592

Data Correlations-4.0% bentonite by weight

Table F.4 Data correlations for 0.60 cm dia. tube

$\dot{\gamma}$ (s^{-1})	τ_w (Pa)	μ_a (Pa·s) $*10^3$	C_f	$Re*10^{-3}$	Q/L (W/m)
100	4.26	42.61	1.0980	0.012	0.007
200	4.81	24.06	0.3100	0.044	0.016
400	6.03	15.08	0.0972	0.141	0.040
600	7.18	11.97	0.0514	0.266	0.072
800	8.38	10.47	0.0337	0.406	0.111
1000	9.58	9.58	0.0247	0.555	0.159
1200	10.68	8.90	0.0191	0.717	0.213
1400	11.87	8.48	0.0156	0.877	0.276
1600	13.05	8.15	0.0131	1.043	0.347
1800	14.24	7.91	0.0113	1.209	0.426
2000	15.32	7.66	0.0099	1.387	0.509
2200	16.45	7.47	0.0088	1.564	0.601
2400	17.72	7.38	0.0079	1.728	0.707
2600	19.15	7.37	0.0073	1.876	0.828
2800	20.59	7.35	0.0068	2.023	0.958
3000	22.07	7.36	0.0063	2.167	1.101

Table F.5 Data correlations for 1.27 cm dia. tube

$\dot{\gamma}$ (s^{-1})	τ_w (Pa)	μ_a (Pa·s) $*10^3$	C_f	$Re*10^{-3}$	Q/L (W/m)
100	4.26	42.61	0.3339	0.048	0.027
200	4.81	24.06	0.0994	0.170	0.065
400	6.03	15.08	0.0326	0.541	0.170
600	7.18	11.97	0.0178	1.023	0.313
800	8.38	10.47	0.0119	1.559	0.496
1000	9.58	9.58	0.0090	2.131	0.734
1200	10.68	8.90	0.0079	2.753	1.119
1400	11.87	8.48	0.0075	3.369	1.688
1600	13.05	8.15	0.0073	4.004	2.446
1800	14.24	7.91	0.0072	4.642	3.412
2000	15.32	7.66	0.0071	5.328	4.586
2200	16.45	7.47	0.0070	6.007	6.019
2400	17.72	7.38	0.0069	6.637	7.705
2600	19.15	7.37	0.0067	7.204	9.653
2800	20.59	7.35	0.0067	7.772	11.984

Table F.6 Data correlations for 1.74 cm dia. tube

$\tilde{\gamma}$ (s^{-1})	τ_w (Pa)	μ_a (Pa·s) $*10^3$	C_f	$Re*10^{-3}$	Q/L (W/m)
100	4.26	42.61	0.1792	0.089	0.051
200	4.81	24.06	0.0553	0.317	0.126
400	6.03	15.08	0.0197	1.010	0.358
600	7.18	11.97	0.0117	1.910	0.685
800	8.38	10.47	0.0077	2.911	1.119
1000	9.58	9.58	0.0065	3.979	1.837
1200	10.68	8.90	0.0069	5.139	3.390
1400	11.87	8.48	0.0078	6.290	6.089

Data Correlations-5.0% bentonite by weight

Table F.7 Data correlations for 0.60 cm dia. tube

$\dot{\gamma}$ (s^{-1})	τ_w (Pa)	μ_a (Pa·s) $*10^3$	C_f	$Re*10^{-3}$	Q/L (W/m)
200	8.76	43.81	0.7656	0.021	0.025
400	11.44	28.61	0.2499	0.064	0.065
600	13.79	22.98	0.1338	0.119	0.118
800	15.75	19.69	0.0860	0.186	0.179
1000	17.59	17.60	0.0615	0.260	0.250
1200	19.15	15.96	0.0465	0.344	0.327
1400	20.61	14.72	0.0367	0.435	0.411
1600	22.02	13.76	0.0301	0.532	0.501
1800	23.46	13.03	0.0253	0.632	0.601
2000	24.90	12.45	0.0217	0.735	0.709
2200	26.33	11.97	0.0190	0.841	0.824
2400	27.77	11.57	0.0168	0.950	0.948
2600	29.13	11.21	0.0151	1.062	1.078

Table F.8 Data correlations for 1.27 cm dia. tube

$\dot{\gamma}$ (s^{-1})	τ_w (Pa)	μ_a (Pa·s) $*10^3$	C_f	$Re*10^{-3}$	Q/L (W/m)
200	8.76	43.81	0.2040	0.094	0.134
400	11.44	28.61	0.0570	0.287	0.300
600	13.79	22.98	0.0320	0.536	0.536
800	15.79	19.69	0.0200	0.834	0.825
1000	17.59	17.60	0.0140	1.167	1.151
1200	19.15	15.96	0.0110	1.544	1.509
1400	20.61	14.72	0.0086	1.953	1.932
1600	22.02	13.76	0.0073	2.387	2.460
1800	23.46	13.03	0.0067	2.837	3.224
2000	24.90	12.45	0.0067	3.300	4.390
2200	26.33	11.97	0.0070	3.775	6.137
2400	27.77	11.57	0.0074	4.261	8.401
2600	29.13	11.21	0.0074	4.766	10.651

Table F.9 Data correlations for 1.74 cm dia. tube

$\dot{\gamma}$ (s^{-1})	τ_w (Pa)	μ_a (Pa·s) $*10^3$	C_f	$Re*10^{-3}$	Q/L (W/m)
200	8.76	43.81	0.1094	0.175	0.250
400	11.44	28.61	0.0362	0.536	0.662
600	13.79	22.98	0.0194	1.001	1.199
800	15.79	19.69	0.0127	1.558	1.861
1000	17.59	17.60	0.0096	2.179	2.740
1200	19.15	15.96	0.0079	2.883	3.880
1400	20.61	14.72	0.0067	3.647	5.290
1600	22.02	13.76	0.0060	4.458	6.986

Data Correlations-6.0% bentonite by weight

Table F.10 Data correlations for 0.60 cm dia. tube

$\dot{\gamma}$ (s^{-1})	τ_w (Pa)	μ_a (Pa-s) $*10^3$	C_f	$Re*10^{-3}$	Q/L (W/m)
207	17.41	84.00	1.4171	0.011	0.051
400	21.88	54.70	0.4791	0.033	0.124
600	25.45	42.41	0.2475	0.064	0.217
800	28.63	35.79	0.1566	0.101	0.326
1000	31.36	31.36	0.1097	0.144	0.446
1200	33.95	28.29	0.0854	0.194	0.580
1500	37.35	24.90	0.0510	0.276	0.797
2000	42.85	21.43	0.0375	0.426	1.220
2500	48.31	19.32	0.0270	0.592	1.719
3000	53.77	17.92	0.0209	0.765	2.295
3500	59.28	16.93	0.0169	0.945	2.952

Table F.11 Data correlations for 1.27 cm dia. tube

$\dot{\gamma}$ (s^{-1})	τ_w (Pa)	μ_a (Pa·s) $*10^3$	C_f	$Re*10^{-3}$	Q/L (W/m)
200	17.41	84.00	0.3006	0.049	0.197
400	21.88	54.70	0.0933	0.150	0.489
600	25.45	42.41	0.0486	0.290	0.859
800	28.63	35.79	0.0309	0.458	1.296
1000	31.36	31.36	0.0216	0.654	1.767
1200	33.95	28.29	0.0163	0.870	2.300
1500	37.35	24.90	0.0118	1.236	3.260
2000	42.85	21.43	0.0088	1.914	5.738
2500	48.31	19.32	0.0065	2.653	8.296

Table F.12 Data correlations for 1.74 cm dia. tube

$\dot{\gamma}$ (s^{-1})	τ_w (Pa)	μ_a (Pa·s) $*10^3$	C_f	$Re*10^{-3}$	Q/L (W/m)
200	17.41	84.00	0.1551	0.091	0.354
400	21.88	54.70	0.0482	0.279	0.879
600	25.45	42.41	0.0250	0.542	1.541
800	28.63	35.79	0.0163	0.856	2.374
1000	31.36	31.36	0.0119	1.221	3.407
1200	33.95	28.29	0.0094	1.624	4.647

Data Correlations-8.0% bentonite by weight

Table F.13 Data correlations for 0.60 cm dia. tube

$\dot{\gamma}$ (s^{-1})	τ_w (Pa)	μ_a (Pa·s) $*10^3$	C_f	$Re*10^{-3}$	Q/L (W/m)
200	22.07	110.36	1.9167	0.008	6.28
300	24.90	82.99	0.9607	0.017	10.63
400	27.41	68.53	0.5949	0.027	15.60
500	29.83	59.66	0.4143	0.038	21.22
600	32.22	53.70	0.3108	0.051	27.51
700	34.35	49.08	0.2434	0.065	32.22
800	36.39	45.48	0.1974	0.081	41.43
1000	40.12	40.12	0.1393	0.115	57.10
1200	43.47	36.23	0.1048	0.153	74.24
1400	46.44	33.17	0.0823	0.194	92.53
1600	49.32	30.82	0.0669	0.239	112.29
1800	52.28	29.05	0.0560	0.285	133.93
2200	58.15	26.43	0.0417	0.383	182.06
2600	64.06	24.64	0.0329	0.486	237.04
3000	69.90	23.30	0.0270	0.593	298.44

Table F.14 Data correlations for 1.27 cm dia. tube

$\dot{\gamma}$ (s^{-1})	τ_w (Pa)	μ_a (Pa·s) $*10^3$	C_f	$Re*10^{-3}$	Q/L (W/m)
200	22.07	110.36	0.4057	0.037	26.70
300	24.90	82.99	0.2062	0.075	45.95
400	27.41	68.53	0.1291	0.120	68.05
500	29.83	59.66	0.0893	0.173	92.17
600	32.22	53.70	0.0668	0.231	119.05
700	34.35	49.08	0.0524	0.303	147.87
800	36.39	45.48	0.0425	0.364	179.76
1000	40.12	40.12	0.0302	0.515	249.16
1200	43.47	36.23	0.0229	0.685	326.50
1400	46.44	33.17	0.0181	0.872	410.88
1600	49.32	30.82	0.0148	1.073	500.39
1800	52.28	29.05	0.0126	1.281	605.32

Table F.15 Data correlations for 1.74 cm dia. tube

$\dot{\gamma}$ (s^{-1})	τ_w (Pa)	μ_a (Pa·s) $*10^3$	C_f	$Re*10^{-3}$	Q/L (W/m)
200	22.07	110.36	0.2422	0.070	55.71
300	24.90	82.99	0.1232	0.139	95.64
400	27.41	68.53	0.0772	0.225	142.03
500	29.83	59.66	0.0542	0.323	194.80
600	32.22	53.70	0.0409	0.431	254.14
700	34.35	49.08	0.0324	0.550	319.68
800	36.39	45.48	0.0268	0.679	395.03

APPENDIX G

NUMERICAL DATA FOR GENERALIZED BINGHAM PLASTIC EQUATION

Values of $\tau_w - \tau_y$ are tabulated for corresponding values of $\dot{\gamma}$ taken from the shear diagram data for all concentrations for the 0.60 cm diameter tube. The values of τ_y are obtained from Figs. 4.3 to 4.7 by extrapolation of the curves to zero $\dot{\gamma}$.

Table G.1 1.96% bentonite by weight. τ_y is 1.0 Pa

$\dot{\gamma}$ (s^{-1})	$\tau_w - \tau_y$ (Pa)
437.0	0.867
1217.6	3.357
1629.4	4.554
2057.2	7.092
2511.3	12.789
3115.9	18.727
3511.1	25.765
4068.8	35.197
4745.7	44.869
5406.4	62.202
5963.6	74.890

Table G.2 4.0% bentonite by weight. τ_y is 3.5 Pa

$\dot{\gamma}$ (s^{-1})	$\tau_w - \tau_y$ (Pa)
264.2	1.384
781.8	4.783
1468.0	8.422
1701.8	9.858
2273.3	13.450
2862.1	17.376
3399.6	21.924
3849.7	33.033
4168.6	39.256
4684.6	59.798
5189.4	75.454

Table G.3 5.0% bentonite by weight. τ_y is 7.0 Pa

$\dot{\gamma}$ (s^{-1})	$\tau_w - \tau_y$ (Pa)
211.9	1.920
1265.2	12.703
2669.8	22.561
3832.8	30.801
5351.7	42.944
6358.5	51.624
7619.3	64.571
8567.1	96.632

Table G.4 6.0% bentonite by weight. τ_y is 11.0 Pa

$\dot{\gamma}$ (s^{-1})	$\tau_w - \tau_y$ (Pa)
207.3	6.414
701.9	16.081
1299.3	23.948
1868.6	30.584
2634.3	39.255
3056.1	43.282
3844.9	50.909

Table G.5 8.0% bentonite by weight. τ_y is 15.0 Pa

$\dot{\gamma}$ (s^{-1})	$\tau_w - \tau_y$ (Pa)
442.6	13.379
1076.6	25.780
2057.0	40.590
2279.2	44.611
3086.9	56.140
3524.4	61.963
4278.4	71.173
4927.3	80.181
5714.9	89.786
6475.5	100.075

APPENDIX H

ANALYSIS OF EXPERIMENTAL ERROR

The overall experimental error can be expressed as the sum of the random errors, the systematic errors and the human errors. Although none of these errors can be eliminated, they were all carefully controlled during the course of the experimentation and sufficiently minimized.

The 'most probable' relative errors in the value of wall shear stress, τ_w and the shear rate, $\dot{\gamma}$ are of prime concern because they limit the accuracy of the experimental work as they express the final form of the accumulated data.

H.1 Wall Shear Stress Error ($d\tau_w/\tau_w$)

The wall shear stress is calculated from the equation:

$$\tau_w = a\Delta P/2L$$

which is to say that:

$$\tau_w = f(a, \Delta P, L)$$

therefore:

$$d\tau_w = (\Delta P/2L)\,da + (a/2L)\,d\Delta P + (-a\Delta P/2L^2)\,dL$$

and:

$$d\tau_w/\tau_w = da/a + d\Delta P/\Delta P + (-dL/L)$$

The 'most probable' absolute error in τ_w can be expressed as the square root of the sum of the square of each individual variable deviation, i.e.,

$$\frac{d\tau_w}{\tau_w} = \sqrt{\left(\frac{da}{a}\right)^2 + \left(\frac{d\Delta P}{\Delta P}\right)^2 + \left(\frac{dL}{L}\right)^2}$$

Particular values of each component in this equation can be estimated as follows.

a) Test section radius errors (da/a)

$$a = (4v/\pi L)^{0.5}/2$$

i.e.,

$$\frac{da}{a} = \frac{1}{2}\sqrt{\left(\frac{dv}{v}\right)^2 + \left(\frac{dL}{L}\right)^2}$$

The volume of Hg used to determine test section radii ranged from 8.0 cm^3 to 80.0 cm^3 and could be measured to an accuracy of ± 0.25 cm^3. Temperature effects were negligible, as tests were completed in a short time interval. The relative errors in volume measurement ranged from a minimum of 0.31% in the 1.74 cm diameter tube to a maximum of 3.1% in the 0.60 cm diameter tube.

The height of the Hg column in the tubes ranged from 21.70 cm to 66.60 cm and could be measured accurately to ± 0.01 cm. The relative errors in height measurements ranged from a minimum of 0.01% in the 0.60 cm diameter tube to a maximum of 0.05% in the 1.74 cm diameter tube.

Thus for each tube, the relative error in the radius could be determined. These errors ranged from a minimum of 0.2% in the 1.27 and 1.74 cm dia. tubes to a maximum of 1.5% in the 0.60 cm dia. tube. From minimum and maximum errors in each tube radius for both sets of data used to determine the radius, the error in the average value of each tube radius was determined.

0.60 cm dia. tube: $\frac{da}{a} = 0.01$

1.27 cm dia. tube: $\frac{da}{a} = 0.002$

1.74 cm dia. tube: $\frac{da}{a} = 0.002$

b) Pressure differential errors ($d\Delta P/\Delta P$)

The final differential pressure (corrected pressure) was determined by subtracting the equivalent head of the pressure transmitting fluid from the pressure differential read from the manometer. Since temperature variations were minimal during the course of the tests, it can be assumed that values of specific gravity for the transmitting fluid and manometer fluid would not change appreciably, so no error was associated with these values or the values used in the conversion of units. Hence the error in the corrected pressure differential is twice the error in the observed pressure differential.

The manometer could be read to ±0.01 inches and the observed pressure drops for all tests ranged from 0.15 inches

to 26.05 inches. The errors in the corrected pressure differentials ranged from a minimum of 0.08% to a maximum of 13.4%.

c) Test section length errors (dL/L)

The distance between pressure taps for each test section was measured to the nearest 0.1 cm.

0.60 cm dia. tube: $\frac{dL}{L} = \frac{0.1}{76.2} = 0.0013$

1.27 cm dia. tube: $\frac{dL}{L} = \frac{0.1}{101.6} = 0.001$

1.74 cm dia. tube: $\frac{dL}{L} = \frac{0.1}{127.0} = 0.0008$

Hence the minimum and maximum errors for τ_w for each tube are:

0.60 cm dia. tube:

$\left(\frac{d\tau_w}{\tau_w}\right)_{min} = \pm 0.35\%$ $\left(\frac{d\tau_w}{\tau_w}\right)_{max} = \pm 6.6\%$

1.27 cm dia. tube:

$\left(\frac{d\tau_w}{\tau_w}\right)_{min} = \pm 0.3\%$ $\left(\frac{d\tau_w}{\tau_w}\right)_{max} = \pm 13.4\%$

1.74 cm dia. tube:

$\left(\frac{d\tau_w}{\tau_w}\right)_{min} = \pm 0.2\%$ $\left(\frac{d\tau_w}{\tau_w}\right)_{max} = \pm 4.6\%$

H.2 Shear Rate Error ($d\dot{\gamma}/\dot{\gamma}$)

Shear rate is calculated from the equation:

$$\dot{\gamma} = 4q/\pi a^3$$

The relative error in $\dot{\gamma}$ can therefore be expressed as:

$$\frac{d\dot{\gamma}}{\dot{\gamma}} = \sqrt{\left(\frac{dq}{q}\right)^2 + 9\left(\frac{da}{a}\right)^2}$$

Since da/a has been determined for each test section radius, it is only necessary to determine dq/q values. The volumetric flow rate for each test was determined by collecting a known volume of the material pumped over a known time interval, thus:

$$\frac{dq}{q} = \sqrt{\left(\frac{dv}{v}\right)^2 + \left(\frac{dt}{t}\right)^2}$$

The volume of material collected could be read from the collection cylinder to the nearest 10.0 cm^3. An additional error of ±5.0 cm^3 was added on to compensate for movement of the collection cylinder while the stop watch was being operated. The maximum volume of material collected for all tests was 3288 cm^3 and the minimum volume was 192 cm^3. Thus the relative error in measuring a volume ranged from 0.46% to 7.8%. A maximum and minimum error for measuring volume was associated with the data for each tube.

The stop watch could be read accurately to ±0.05 seconds and an additional 0.05 seconds was allowed for human error in operating it. The minimum time for which a sample was collected was 1.80 seconds and the maximum time was 57.20

seconds. These correspond to a range of timing errors lying between 0.17% and 5.5%.

From these errors, an overall minimum and maximum error for the measurement of flow rate in each tube was established for use in the calculation of shear rate error. The minimum error in measuring the flow rate was about 0.6% and the maximum was 8.0%.

A minimum and maximum error for $\dot{\gamma}$ in each tube is given below.

0.60 cm dia. tube:

$$\left(\frac{d\dot{\gamma}}{\dot{\gamma}}\right)_{min} = \pm 3.4\% \qquad \left(\frac{d\dot{\gamma}}{\dot{\gamma}}\right)_{max} = \pm 8.5\%$$

1.27 cm dia. tube:

$$\left(\frac{d\dot{\gamma}}{\dot{\gamma}}\right)_{min} = \pm 0.8\% \qquad \left(\frac{d\dot{\gamma}}{\dot{\gamma}}\right)_{max} = \pm 6.1\%$$

1.74 cm dia. tube:

$$\left(\frac{d\dot{\gamma}}{\dot{\gamma}}\right)_{min} = \pm 1.0\% \qquad \left(\frac{d\dot{\gamma}}{\dot{\gamma}}\right)_{max} = \pm 5.9\%$$

H.3 Apparent Viscosity Error ($d\mu_a/\mu_a$)

Apparent viscosity is calculated from:

$$\mu_a = \tau_w/\dot{\gamma}$$

Thus:

$$\frac{d\mu_a}{\mu_a} = \sqrt{\left(\frac{d\tau_w}{\tau_w}\right)^2 + \left(\frac{d\dot{\gamma}}{\dot{\gamma}}\right)^2}$$

0.60 cm dia. tube:

$$\left(\frac{d\mu_a}{\mu_a}\right)_{min} = \pm 3.4\% \qquad \left(\frac{d\mu_a}{\mu_a}\right)_{max} = \pm 9.1\%$$

1.27 cm dia. tube:

$$\left(\frac{d\mu_a}{\mu_a}\right)_{min} = \pm 1.0\% \qquad \left(\frac{d\mu_a}{\mu_a}\right)_{max} = \pm 9.1\%$$

1.74 cm dia. tube:

$$\left(\frac{d\mu_a}{\mu_a}\right)_{min} = \pm 1.0\% \qquad \left(\frac{d\mu_a}{\mu_a}\right)_{max} = \pm 6.3\%$$

H.4 Friction Factor Error (dC_f/C_f)

The friction factor is calculated from:

$$C_f = 2\tau_w/\rho u_m^2$$

and,

$$\frac{dC_f}{C_f} = \sqrt{\left(\frac{d\tau_w}{\tau_w}\right)^2 + \left(\frac{d\rho}{\rho}\right)^2 + 4\left(\frac{du_m}{u_m}\right)^2}$$

The density of each fluid was determined by weighing a known volume. The weight of each sample could be measured to ±0.005E-03 kg. Since each sample tested weighed about 10.00E-03 kg, the error in weight for all samples was about 0.05%.

The volume of the sample to be weighed could be read to the nearest 0.01 cm^3 and since each sample was about 10.0

cm^3, the relative error is 0.1%.

Thus the relative error in density was ±0.1%.

The average velocity for the flow in each tube was found by dividing q_{avg} by the cross sectional area of the tube, i.e.,

$$u_m = q/\alpha$$

Since:

$$\alpha = \pi a^2$$

then,

$$\frac{du_m}{u_m} = \sqrt{\left(\frac{dq}{q}\right)^2 + 4\left(\frac{da}{a}\right)^2}$$

Since dq/q and da/a have been determined, du_m/u_m was easily found and ranged from 0.8% to 8.2% for all three tubes.

The friction factor error for each tube was as follows:

0.60 cm dia. tube:

$$\left(\frac{dC_f}{C_f}\right)_{min} = \pm 5.2\% \qquad \left(\frac{dC_f}{C_f}\right)_{max} = \pm 17.0\%$$

1.27 cm dia. tube:

$$\left(\frac{dC_f}{C_f}\right)_{min} = \pm 1.4\% \qquad \left(\frac{dC_f}{C_f}\right)_{max} = \pm 14.0\%$$

1.74 cm dia. tube:

$$\left(\frac{dC_f}{C_f}\right)_{min} = \pm 1.6\% \qquad \left(\frac{dC_f}{C_f}\right)_{max} = \pm 12.0\%$$

H.5 Reynolds Number Error (dRe/Re)

The Reynolds number is calculated from:

$$Re = 2\rho a u_m/\mu_a$$

Thus:

$$\frac{dRe}{Re} = \sqrt{\left(\frac{d\rho}{\rho}\right)^2 + \left(\frac{da}{a}\right)^2 + \left(\frac{du_m}{u_m}\right)^2 + \left(\frac{d\mu_a}{\mu_a}\right)^2}$$

0.60 cm dia. tube:

$$\left(\frac{dRe}{Re}\right)_{min} = \pm 4.4\% \qquad \left(\frac{dRe}{Re}\right)_{max} = \pm 12.3\%$$

1.27 cm dia. tube:

$$\left(\frac{dRe}{Re}\right)_{min} = \pm 1.1\% \qquad \left(\frac{dRe}{Re}\right)_{max} = \pm 10.9\%$$

1.74 cm dia. tube:

$$\left(\frac{dRe}{Re}\right)_{min} = \pm 1.3\% \qquad \left(\frac{dRe}{Re}\right)_{max} = \pm 8.6\%$$

H.6 Power Consumption Error (d(Q/L)/(Q/L)

The power required to pump the material for each unit length of tube was found from the equation:

$$Q/L = q\Delta P/L$$

Therefore:

$$\frac{d(Q/L)}{Q/L} = \sqrt{\left(\frac{dq}{q}\right)^2 + \left(\frac{d\Delta P}{\Delta P}\right)^2 + \left(\frac{dL}{L}\right)^2}$$

0.60 cm dia. tube:

$$\left(\frac{d(Q/L)}{Q/L}\right)_{min} = \pm 1.6\% \qquad \left(\frac{d(Q/L)}{Q/L}\right)_{max} = \pm 8.6\%$$

1.27 cm dia. tube:

$$\left(\frac{d(Q/L)}{Q/L}\right)_{min} = \pm 0.6\% \qquad \left(\frac{d(Q/L)}{Q/L}\right)_{max} = \pm 9.1\%$$

1.74 cm dia. tube:

$$\left(\frac{d(Q/L)}{Q/L}\right)_{min} = \pm 0.7\% \qquad \left(\frac{d(Q/L)}{Q/L}\right)_{max} = \pm 6.3\%$$